7-19-2022

Green, Quantized Federated Learning over Wireless Networks: An Energy-Efficient Design

Minsu Kim

Walid Saad

Mohammad Mozaffari

Mérouane Debbah

Green, Quantized Federated Learning over Wireless Networks: An Energy-Efficient Design

Minsu Kim, Walid Saad, *Fellow, IEEE*, Mohammad Mozaffari, *Member IEEE*, and Merouane Debbah, *Fellow, IEEE*

Abstract

The practical deployment of federated learning (FL) over wireless networks requires balancing energy efficiency and convergence time due to the limited available resources of devices. Prior art on FL often trains deep neural networks (DNNs) to achieve high accuracy and fast convergence using 32 bits of precision level. However, such scenarios will be impractical for resource-constrained devices since DNNs typically have high computational complexity and memory requirements. Thus, there is a need to reduce the precision level in DNNs to reduce the energy expenditure. In this paper, a green-quantized FL framework, which represents data with a finite precision level in both local training and uplink transmission, is proposed. Here, the finite precision level is captured through the use of quantized neural networks (QNNs) that quantize weights and activations in fixed-precision format. In the considered FL model, each device trains its QNN and transmits a quantized training result to the base station. Energy models for the local training and the transmission with quantization are rigorously derived. To minimize the energy consumption and the number of communication rounds simultaneously, a multi-objective optimization problem is formulated with respect to the number of local iterations, the number of selected devices, and the precision levels for both local training and transmission while ensuring convergence under a target accuracy constraint. To solve this problem, the convergence rate of the proposed FL system is analytically derived with respect to the system control variables. Then, the Pareto boundary of the problem is characterized to provide efficient solutions using the normal boundary inspection method. Design insights on balancing the tradeoff between the two objectives are

M. Kim and W. Saad are with the Wireless@VT Group, Bradley Department of Electrical and Computer Engineering, Virginia Tech, Arlington, VA, USA (email: {msukim, walids}@vt.edu.)

M. Mozaffari is with Ericsson Research, Santa Clara, CA, USA (email: mohammad.mozaffari@ericsson.com).

M. Debbah is with Technology Innovation Institute and Mohamed Bin Zayed University of Artificial Intelligence, Abu Dhabi, United Arab Emirates (email: merouane.debbah@tii.ae).

A preliminary version of this work was presented at IEEE ICC 2022 [1].

This research was supported by the U.S. National Science Foundation under Grant CNS-2114267.

drawn from using the Nash bargaining solution and analyzing the derived convergence rate. Simulation results show that the proposed FL framework can reduce energy consumption until convergence by up to 52% compared to a baseline FL algorithm that represents data with full precision.

I. Introduction

Federated learning (FL) is an emerging paradigm that enables distributed learning among wireless devices [2]. In FL, a central server (e.g., a base station (BS)) and multiple mobile devices collaborate to train a shared machine learning model without sharing raw data. Many FL works employ deep neural networks (DNNs), whose size constantly grows to match the increasing demand for higher accuracy [3]. Such DNN architectures can have tens of millions of parameters and billions of multiply-accumulate (MAC) operations. Moreover, to achieve fast convergence, these networks typically represent data in 32 bits of full precision level, which may consume significant energy due to high computational complexity and memory requirements [4]. Additionally, a large DNN can induce a significant communication overhead [5]. Under such practical constraints, it may be challenging to deploy FL over resource-constrained Internet of Things (IoT) devices due to its large energy cost. To design an energy-efficient, green FL scheme, one can reduce the precision level to decrease the energy consumption during the local training and communication phase. However, a low precision level can jeopardize the convergence rate by introducing quantization errors. Therefore, finding the optimal precision level that balances energy efficiency and convergence rate while meeting desired FL accuracy constraints will be a major challenge for the practical deployment of green FL over wireless networks.

Several works have studied the energy efficiency of FL from a system-level perspective [6]–[11]. The work in [6] investigated the energy efficiency of FL algorithms in terms of the carbon footprint compared to centralized learning. In [7], the authors formulated a joint minimization problem for energy consumption and training time by optimizing heterogeneous computing and wireless resources. The work in [8] developed an approach to minimize the total energy consumption by controlling a target accuracy during local training based on a derived convergence rate. The authors in [9] proposed a sum energy minimization problem by considering joint bandwidth and workload allocation of heterogeneous devices. In [10], the authors studied a joint optimization problem whose goal is to minimize the energy consumption and the training time while achieving a target accuracy. The work in [11] developed a resource management scheme by leveraging the information of loss functions of each device to maximize the accuracy under

constrained communication and computation resources. However, these works [6]–[11] did not consider the energy efficiency of their DNN structure during training. Since mobile devices have limited computing and memory resources, deploying an energy-efficient DNN will be necessary for green FL.

To further improve FL energy efficiency, model compression methods such as quantization were studied in [12]–[15]. The work in [12] proposed a quantization scheme for both uplink and downlink transmission in FL and analyzed the impact of the quantization on the convergence rate. In [13], the authors proposed an FL scheme with periodic averaging and quantized model uploading to improve the communication efficiency. The authors in [14] and [15] considered a novel FL setting, in which each device trains a ternary/binary neural network so as to alleviate the communication overhead by uploading ternary/binary parameters to the server. However, the works in [12] and [13] only considered the communication efficiency while there can be a large energy consumption in training. Although the works in [14] and [15], considered ternary/binarized neural networks during local training, they did not optimize the quantization levels of the neural network to balance the tradeoff between energy efficiency and convergence rate. To the best of our knowledge, there is no work that jointly considers the tradeoff between energy efficiency and convergence rate while controlling the optimal precision level for green FL over wireless networks.

The main contribution of this paper is a novel green, energy-efficient quantized FL framework that can represent data with a finite precision level in both local training and uplink transmission. In our FL model, all devices train their quantized neural network (QNN), whose weights and activations are quantized with a finite precision level, so as to decrease energy consumption for computation and memory access. After training, each device calculates the training result and transmits its quantized version to the BS. The BS then aggregates the received information to generate a new global model and transmits it back to the devices. To quantify the energy consumption, we propose a rigorous energy model for the local training based on the physical structure of a processing chip. We also derive the energy model for the uplink transmission with quantization. Although a low precision level can save the energy consumption per iteration, it decreases the convergence rate because of quantization errors. Thus, there is a need for a new approach to analyze the tradeoff between energy efficiency and convergence rate by optimizing the precision levels while meeting target accuracy constraints. To this end, we formulate a multi-objective optimization problem by controlling the precision levels to minimize the total energy

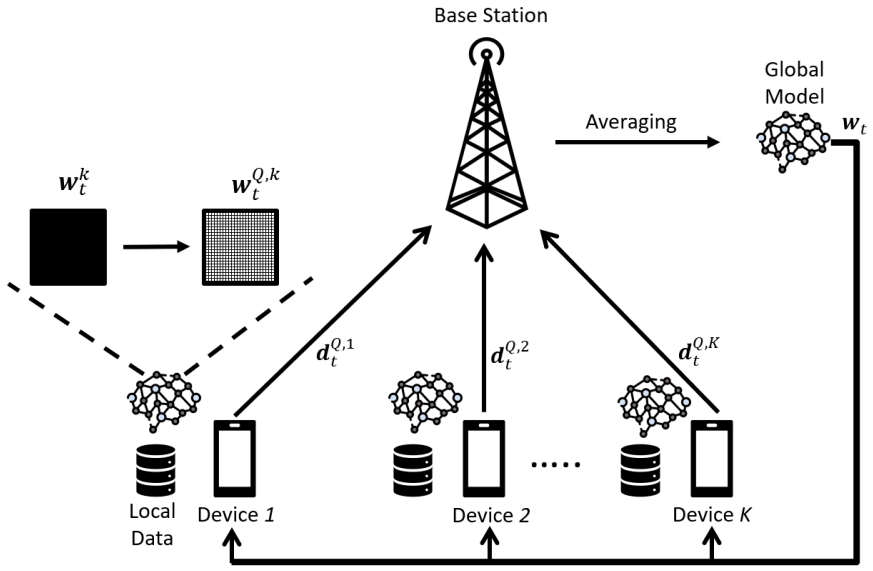

Fig. 1: An illustration of the quantized FL model over wireless network.

consumption and the number of communication rounds while ensuring convergence with a target accuracy. We also incorporate two additional control variables: the number of local iterations and the number of selected devices at each communication round, which have a significant impact on both the energy consumption and the convergence time. To solve this problem, we first analytically derive the convergence rate of our FL framework with respect to the control variables. Then, we use the normal boundary inspection (NBI) method to obtain the Pareto boundary of our multi-objective optimization problem. To balance the tradeoff between the two objectives, we present and analyze two practical operating points: the Nash bargaining solution (NBS) and the sum minimizing solution (SUM) points. Based on these two operating points and the derived convergence rate, we provide design insights into the proposed FL framework. For instance, the total energy consumption until convergence initially decreases as the precision level increases, however, after a certain threshold, higher precision will mean higher energy costs. Meanwhile, the convergence rate will always improve with a higher precision. We also provide the impacts of system parameters such as the number of devices and model size on the performance of the proposed FL. Simulation results show that our FL model can reduce the energy consumption by up to 52% compared to a baseline that represents data in full precision.

The rest of this paper is organized as follows. Section II presents the system model. In Section III, we describe the studied problem. Section III-D introduces NBS. Section IV provides simulation results. Finally, conclusions are drawn in Section V.

II. System Model

Consider an FL system having N devices connected to a BS as shown in Fig. 1. Each device k has its own local dataset $\mathcal{D}_k = \{\boldsymbol{x}_{kl}, \boldsymbol{y}_{kl}\}$, where $l = 1, \ldots, D_k$. For example, $\{\boldsymbol{x}_{kl}, \boldsymbol{y}_{kl}\}$ can be an input-output pair for image classification, where $\boldsymbol{x}_{kl}$ is an input vector and $\boldsymbol{y}_{kl}$ is the corresponding output. We define a loss function $f(\boldsymbol{w}^k, \boldsymbol{x}_{kl}, \boldsymbol{y}_{kl})$ to quantify the performance of a machine learning (ML) model with parameters $\boldsymbol{w}^k \in \mathbb{R}^d$ over $\{\boldsymbol{x}_{kl}, \boldsymbol{y}_{kl}\}$, where d is the number of parameters. Since device k has D_k data samples, its local loss function can be given by $F_k(\boldsymbol{w}^k) = \frac{1}{D_k}\sum_{l=1}^{D_k} f(\boldsymbol{w}^k, \boldsymbol{x}_{kl}, \boldsymbol{y}_{kl})$. The FL process aims to find the global parameters $\boldsymbol{w}$ that can solve the following optimization problem:

$$\min_{\boldsymbol{w}^1,\ldots,\boldsymbol{w}^N} F(\boldsymbol{w}) = \sum_{k=1}^{N} \frac{D_k}{D} F_k(\boldsymbol{w}^k) = \frac{1}{D}\sum_{k=1}^{N}\sum_{l=1}^{D_k} f(\boldsymbol{w}^k, \boldsymbol{x}_{kl}, \boldsymbol{y}_{kl}) \tag{1}$$

$$\text{s.t.} \quad \boldsymbol{w}^1 = \boldsymbol{w}^2 = \cdots = \boldsymbol{w}^N = \boldsymbol{w}, \tag{2}$$

where $D = \sum_{k=1}^{N} D_k$ is the total size of the entire dataset $\mathcal{D} = \cup_{k=1}^{N} \mathcal{D}_k$. We assume that the local datasets are identically distributed in order to guarantee that the expected stochastic gradient from $\mathcal{D}_k$ equals to the one from $\mathcal{D}$ for all $k \in \{1, \ldots, N\}$ [14], [16].

Solving problem (2) typically requires an iterative process between the BS and devices. However, in practical systems, such as IoT systems, these devices are resource-constrained, particularly when it comes to computing and energy. Hence, we propose to manage the precision level of parameters used in our FL algorithm to reduce the energy consumption for computation, memory access, and transmission. As such, we adopt a QNN architecture whose weights and activations are quantized in fixed-point format rather than conventional 32-bit floating-point format [17]. During the training time, a QNN can reduce the energy consumption for MAC operation and memory access due to quantized weights and activations.

A. Quantized Neural Networks

In our model, each device trains a QNN of identical structure using n bits for quantization. High precision can be achieved if we increase n at the cost of more energy usage. We can represent any given number in a fixed-point format such as $[\Omega.\Phi]$, where Ω is the integer part and Φ is the fractional part of the given number [18]. Here, we use one bit to represent the integer part and $(n-1)$ bits for the fractional part. Then, the smallest positive number that we can present is $\kappa = 2^{-n+1}$, and the possible range of numbers with n bits will be $[-1, 1-2^{-n+1}]$.

Note that a QNN restricts the value of weights to [-1, 1]. Otherwise, weights can be very large without meaningful impact on the performance. We consider a stochastic quantization scheme [18] since it generally performs better than deterministic quantization [19]. Any given number $w \in \boldsymbol{w}$ can be stochastically quantized as follows:

$$Q(w) = \begin{cases} \lfloor w \rfloor, & \text{with probability} \quad \frac{\lfloor w \rfloor + \kappa - w}{\kappa}, \\ \lfloor w \rfloor + \kappa, & \text{with probability} \quad \frac{w - \lfloor w \rfloor}{\kappa}, \end{cases} \tag{3}$$

where $\lfloor w \rfloor$ is the largest integer multiple of κ less than or equal to w. In the following lemma, we analyze the features of the stochastic quantization.

Lemma 1. *For the stochastic quantization $Q(\cdot)$, a scalar w, and a vector $\boldsymbol{w} \in \mathbb{R}^d$, we have*

$$\mathbb{E}[Q(w)] = w, \quad \mathbb{E}[(Q(w) - w)^2] \leq \frac{1}{2^{2n}}, \tag{4}$$

$$\mathbb{E}[Q(\boldsymbol{w})] = \boldsymbol{w}, \quad \mathbb{E}[||Q(\boldsymbol{w}) - \boldsymbol{w}||^2] \leq \frac{d}{2^{2n}}. \tag{5}$$

Proof. We first derive $\mathbb{E}[Q(w)]$ as

$$\mathbb{E}[Q(w)] = \lfloor w \rfloor \frac{\lfloor w \rfloor + \kappa - w}{\kappa} + (\lfloor w \rfloor + \kappa) \frac{w - \lfloor w \rfloor}{\kappa} = w. \tag{6}$$

Similarly, $\mathbb{E}[(Q(w) - w)^2]$ can be obtained as

$$\begin{aligned} \mathbb{E}[(Q(w) - w)^2] &= (\lfloor w \rfloor - w)^2 \frac{\lfloor w \rfloor + \kappa - w}{\kappa} + (\lfloor w \rfloor + \kappa - w)^2 \frac{w - \lfloor w \rfloor}{\kappa} \\ &= (w - \lfloor w \rfloor)(\lfloor w \rfloor + \kappa - w) \leq \frac{\kappa^2}{4} = \frac{1}{2^{2n}}, \end{aligned} \tag{7}$$

where (7) follows from the arithmetic mean and geometric mean inequality. Since expectation is a linear operator, we have $\mathbb{E}[Q(\boldsymbol{w})] = \boldsymbol{w}$ from (6). From the definition of the square norm, $\mathbb{E}[||Q(\boldsymbol{w}) - \boldsymbol{w}||^2]$ can obtained as

$$\mathbb{E}[||Q(\boldsymbol{w}) - \boldsymbol{w}||^2] = \sum_{j=1}^{d} \mathbb{E}[(Q(w_j) - w_j)^2] \leq \frac{d}{2^{2n}}. \tag{8}$$

□

From Lemma 1, we can see that our quantization scheme is unbiased as its expectation is zero. However, the quantization error can still increase for a large model.

For device k, we denote the quantized weights of layer l as $\boldsymbol{w}_{(l)}^{Q,k} = Q(\boldsymbol{w}_{(l)}^k)$, where $\boldsymbol{w}_{(l)}^k$ is the parameters of layer l. Then, the output of layer l will be: $o_{(l)} = g_{(l)}(\boldsymbol{w}_{(l)}^{Q,k}, o_{(l-1)})$, where $o_{(l-1)}$ is the output from the previous layer $l-1$, and $g(\cdot)$ is the operation of layer l on the input,

including the linear sum of $\boldsymbol{w}_{(l)}^{Q,k}$ and $o_{(l-1)}$, batch normalization, and activation. Note that our activation includes the stochastic quantization after a normal activation function such as ReLU. Then, the output of layer l, i.e., $o_{(l)}$, is fed into the next layer as an input. For training, we use the stochastic gradient descent (SGD) algorithm as follows

$$\boldsymbol{w}_{\tau+1}^{k} \leftarrow \boldsymbol{w}_{\tau}^{k} - \eta \nabla F_k(\boldsymbol{w}_{\tau}^{Q,k}, \xi_{\tau}^{k}), \tag{9}$$

where $\tau = 1 \dots I$ is training iteration, η is the learning rate, and ξ is a sample from D_k for the current update. The update of weights is done in full precision so that SGD noise can be averaged out properly [15]. Then, we restrict the values of $\boldsymbol{w}_{\tau+1}^{k}$ to $[-1, 1]$ as $\boldsymbol{w}_{\tau+1}^{k} \leftarrow \text{clip}(\boldsymbol{w}_{\tau+1}^{k}, -1, 1)$ where $\text{clip}(\cdot, -1, 1)$ projects an input to 1 if it is larger than 1, and projects an input to -1 if it is smaller than -1. Otherwise, it returns the same value as the input. Otherwise, $\boldsymbol{w}_{\tau+1}^{k}$ can become significantly large without a meaningful impact on quantization [17]. After each training, $\boldsymbol{w}_{\tau+1}^{k}$ will be quantized as $\boldsymbol{w}_{\tau+1}^{Q,k}$ for the forward propagation.

B. FL model

For learning, without loss of generality, we adopt FedAvg [4] to solve problem (2). At each communication round t, the BS randomly selects a set of devices $\mathcal{N}_t$ such that $|\mathcal{N}_t| = K$ and transmits the current global model $\boldsymbol{w}_t$ to the scheduled devices. Each device in $\mathcal{N}_t$ trains its local model based on the received global model by running I steps of SGD as below

$$\boldsymbol{w}_{t,\tau}^{k} = \boldsymbol{w}_{t,\tau-1}^{k} - \eta_t \nabla F_k(\boldsymbol{w}_{t,\tau-1}^{Q,k}, \xi_{\tau}^{k}), \forall \tau = 1, \dots, I, \tag{10}$$

where η_t is the learning rate at communication round t. Note that unscheduled devices do not perform local training. Then, each device in $\mathcal{N}_t$ calculates the model update $\boldsymbol{d}_{t+1}^{k} = \boldsymbol{w}_{t+1}^{k} - \boldsymbol{w}_{t}^{k}$, where $\boldsymbol{w}_{t+1}^{k} = \boldsymbol{w}_{t,I-1}^{k}$ and $\boldsymbol{w}_{t}^{k} = \boldsymbol{w}_{t,0}^{k}$ [12]. Typically, $\boldsymbol{d}_{t+1}^{k}$ has millions of elements for DNN. It is not practical to send $\boldsymbol{d}_{t+1}^{k}$ with full precision for energy-constrained devices. Hence, we apply the same quantization scheme used in QNNs to $\boldsymbol{d}_{t+1}^{k}$ by denoting its quantized equivalent as $\boldsymbol{d}_{t+1}^{Q,k}$ with precision level m. Thus, each device in $\mathcal{N}_t$ clips its model update $\boldsymbol{d}_{t+1}^{k}$ using $\text{clip}(\cdot)$ to match the quantization range and transmits its quantized version to the BS. The received model updates are averaged by the BS, and the next global model $\boldsymbol{w}_{t+1}$ will be generated as below

$$\boldsymbol{w}_{t+1} = \boldsymbol{w}_{t} + \frac{1}{K} \sum_{k \in \mathcal{N}_t} \boldsymbol{d}_{t+1}^{Q,k}. \tag{11}$$

The FL system repeats this process until the global loss function converges to a target accuracy constraint ϵ. We summarize this algorithm in Algorithm 1. Next, we propose the energy model for the computation and the transmission of our FL system.

Algorithm 1: Quantized FL Algorithm

Input: K, I, initial model $\boldsymbol{w}_0$, $t = 0$, target accuracy ϵ

repeat

  The BS randomly selects a subset of devices $\mathcal{N}_t$ and transmits $\boldsymbol{w}_t$ to the selected devices;

  Each device $k \in \mathcal{N}_t$ trains its QNN by running I steps of SGD as (9);

  Each device $k \in \mathcal{N}_t$ transmits $\boldsymbol{d}_{t+1}^{Q,k}$ to the BS;

  The BS generates a new global model $\boldsymbol{w}_{t+1} = \boldsymbol{w}_t + \frac{1}{K}\sum_{k\in\mathcal{N}_t} \boldsymbol{d}_{t+1}^{Q,k}$;

  $t \leftarrow t + 1$;

until *target accuracy* ϵ *is satisfied*;

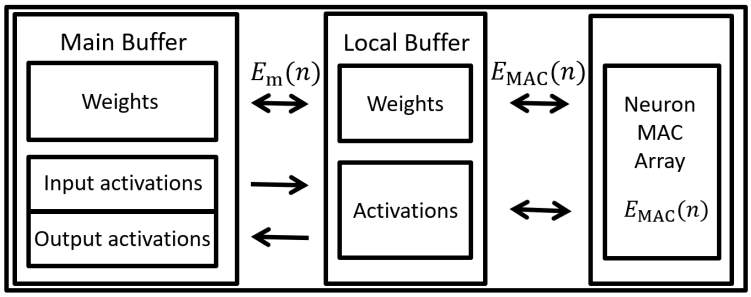

Fig. 2: An illustration of the two-dimensional processing chip.

C. Computing and Transmission model

1) Computing model: We consider a typical two-dimensional processing chip for convolutional neural networks (CNNs) as shown in Fig. 2 [5]. This chip has a parallel neuron array, p MAC units, and two memory levels: a main buffer that stores the current layers' weights and activations and a local buffer that caches currently used weights and activations. We use the MAC operation energy model of [20] whereby $E_{\mathrm{MAC}}(n) = A\,(n/n_{\max})^{\alpha}$ for precision level n, where $A > 0$, $1 < \alpha < 2$, and $n_{\max}$ is the maximum precision level. Here, a MAC operation includes a given layer operation such as output calculation, batch normalization, activation, and weight update. Then, the energy consumption for accessing a local buffer can be modeled as $E_{\mathrm{MAC}}(n)$, and the energy for accessing a main buffer can be given by $E_{\mathrm{m}}(n) = 2E_{\mathrm{MAC}}(n)$ [5] .

The energy consumption of device k for doing inference (i.e., forward propagation) is $E_{\mathrm{inf}}^{k}(n)$ when n bits are used for the quantization. Then, $E_{\mathrm{inf}}^{k}(n)$ is the sum of the computing energy $E_{\mathrm{C}}(n)$, the access energy for fetching weights from the buffers $E_{\mathrm{W}}(n)$, and the access energy for fetching activations from the buffers $E_{\mathrm{A}}(n)$, as follows [20]:

$$E_{\mathrm{inf}}^{k}(n) = E_{\mathrm{C}}(n) + E_{\mathrm{W}}(n) + E_{\mathrm{A}}(n),$$

$$E_{\mathrm{C}}(n) = E_{\mathrm{MAC}}(n)N_c + 2O_s\ E_{\mathrm{MAC}}(n_{\max}),$$

$$E_{\mathrm{W}}(n) = E_{\mathrm{m}}(n)N_s + E_{\mathrm{MAC}}(n)N_c\sqrt{n/pn_{\max}},$$
$$E_{\mathrm{A}}(n) = 2E_{\mathrm{m}}(n)O_s + E_{\mathrm{MAC}}(n)N_c\sqrt{n/pn_{\max}}, \tag{12}$$

where N_c is the number of MAC operations, N_s is the number of weights, and O_s is the number of intermediate outputs in the network. For $E_{\mathrm{C}}(n)$, in a QNN, batch normalization and activation are done in full-precision $n_{\max}$ to each output O_s [17]. Once we fetch weights from a main to a local buffer, they can be reused in the local buffer afterward as shown in $E_{\mathrm{W}}(n)$. In Fig. 2, a MAC unit fetches weights from a local buffer to do computation. Since we are using a two-dimensional MAC array of p MAC units, they can share fetched weights with the same row and column, which has $\sqrt{p}$ MAC units respectively. In addition, a MAC unit can fetch more weights due to the n bits quantization compared with when weights are represented in $n_{\max}$ bits. Thus, we can reduce the energy consumption to access a local buffer by the amount of $\sqrt{n/pn_{\max}}$. A similar process applies to $E_{\mathrm{A}}(n)$ since activations are fetched from the main buffer and should be saved back to it for the calculation in the next layer.

As introduced in Section II-A, we update weights of QNN in full-precision to average out the noise from SGD. Then, the energy consumption to update weights will be

$$E_{\mathrm{up}} = N_c E_{\mathrm{MAC}}(n_{\max}) + 2E_{\mathrm{m}}(n_{\max}) + E_{\mathrm{l}}(n_{\max})N_c\sqrt{\frac{1}{p}}, \tag{13}$$

where we approximate the total number of MAC operations for the weight update to N_c. Note that we need to fetch weights from the main buffer to the local buffer for an update. Then, the neuron MAC array proceeds with the update by fetching the cached weights from the local buffer. Therefore, the energy consumption for one iteration of device k is given by

$$E^{C,k}(n) = E^k_{\mathrm{inf}}(n) + E_{\mathrm{up}},\ k \in \{1, \ldots, N\}. \tag{14}$$

2) Transmission Model: We use the orthogonal frequency domain multiple access (OFDMA) to transmit model updates to the BS. Each device occupies one resource block. The achievable rate of device k will be:

$$r_k = B\log_2\left(1 + \frac{p_k h_k}{N_0 B}\right), \tag{15}$$

where B is the allocated bandwidth, h_k is the channel gain between device k and the BS, p_k is the transmit power of device k, and N_0 is the power spectral density of white noise. After local training, device k normalizes the model update as $\boldsymbol{d}^k_t/||\boldsymbol{d}^k_t||$ to match the predetermined

quantization range $[-1, 1]$. Then, it transmits $\boldsymbol{d}_t^{Q,k}$ to the BS at given communication round t. The transmission time T_k for uploading $\boldsymbol{d}_t^{Q,k}$ is given by

$$T_k(m) = \frac{||\boldsymbol{d}_t^{Q,k}||}{r_k} = \frac{||\boldsymbol{d}_t^k||m}{r_k m_{\text{max}}}. \tag{16}$$

Note that $\boldsymbol{d}_t^{Q,k}$ is quantized with m bits while $\boldsymbol{d}_t^k$ is represented with m_{max} bits. Then, the energy consumption for the uplink transmission is given by

$$E^{UL,k}(m) = T_k(m) \times p_k = \frac{p_k||\boldsymbol{d}_t^k||m}{B\log_2\left(1 + \frac{p_k h_k}{N_0 B}\right) m_{\text{max}}}. \tag{17}$$

III. Time and Energy efficient Federated QNN

Given our model, we now formulate a multi-objective optimization problem to minimize the energy consumption and the number of communication rounds while ensuring convergence under a target accuracy. We show that a tradeoff exists between the energy consumption and the number of communication rounds as a function of I, K, m, and n. For instance, the system can allocate more bits and sample more devices to converge faster, i.e, to reduce the number of communication rounds, at the expense of spending more energy. Conversely, the system may choose slow learning if it prioritizes the minimization of the energy consumption. Hence, finding the optimal solutions is important to balance this tradeoff and to achieve the target accuracy.

We aim to minimize both the expected total energy consumption and the number of communication rounds until convergence under a target accuracy ϵ as follows:

$$\min_{I,K,m,n} \quad \left[\mathbb{E}\left[\sum_{t=1}^{T}\sum_{k\in\mathcal{N}_t} E^{UL,k}(m) + IE^{C,k}(n)\right], T\right] \tag{18a}$$

$$\text{s.t.} \quad I \in [I_{\text{min}}, \ldots, I_{\text{max}}], K \in [K_{\text{min}}, \ldots, N] \tag{18b}$$

$$m \in [1, \ldots, m_{\text{max}}], n \in [1, \ldots, n_{\text{max}}] \tag{18c}$$

$$\mathbb{E}[F(\boldsymbol{w}_T)] - F(\boldsymbol{w}^*) \leq \epsilon, \tag{18d}$$

where I is the number of local iterations, I_{min} and I_{max} denote the minimum and maximum of I, respectively, $\mathbb{E}[F(\boldsymbol{w}_T)]$ is the expectation of global loss function after T communication rounds, $F(\boldsymbol{w}^*)$ is the minimum value of F, and ϵ is the target accuracy. The possible values of I and K are given by (18b). Constraint (18c) represents the maximum precision levels in the transmission and the computation, respectively. Constraints (18d) captures the required number of communication rounds to achieve ϵ.

This problem is challenging to solve since obtaining an analytical expression of (18d) with respect to the control variables is difficult. Hence, deriving the exact T to achieve (18d) is not trivial. Moreover, a global optimal solution, which minimizes each objective function simultaneously, is generally infeasible for a multi-objective optimization problem [21]. Therefore, a closed-form solution may not exist.

To solve this problem, we first obtain the analytical relationship between (18d) and I, K, m, and n to derive T with respect to ϵ. As done in [10], [12], [22], we make the following assumptions on the loss function as follows

Assumption 1. *The loss function has the following properties*

- $F_k(\boldsymbol{w})$ *is L-smooth:* $\forall\ \boldsymbol{v}$ *and* $\boldsymbol{w}\ F_k(\boldsymbol{v}) \leq F_k(\boldsymbol{w}) + (\boldsymbol{v}-\boldsymbol{w})^T \nabla F_k(\boldsymbol{w}) + \frac{L}{2}||\boldsymbol{v}-\boldsymbol{w}||^2$
- $F_k(\boldsymbol{w})$ *is* μ*-strongly convex:* $\forall\ \boldsymbol{v}$ *and* $\boldsymbol{w}\ F_k(\boldsymbol{v}) \geq F_k(\boldsymbol{w}) + (\boldsymbol{v}-\boldsymbol{w})^T \nabla F_k(\boldsymbol{w}) + \frac{\mu}{2}||\boldsymbol{v}-\boldsymbol{w}||^2$
- *The variance of stochastic gradient (SG) is bounded:* $\mathbb{E}[||\nabla F_k(\boldsymbol{w}_t^k, \xi_t^k) - \nabla F_k(\boldsymbol{w}_t^k)||^2] \leq \sigma_k^2,\ \forall k = 1, \ldots, N.$
- *The squared norm of SG is bounded:* $\mathbb{E}[||\nabla F_k(\boldsymbol{w}_t^k, \xi_t^k)||^2] \leq G^2,\ \forall k = 1, \ldots, N.$

These assumptions hold for some practical loss functions. Such examples include logistic regression, l_2 norm regularized linear regression, and softmax classifier [23]. Since we use the quantization in both local training and transmission, the quantization error negatively affects the accuracy and the convergence of our FL system. We next leverage the results of Lemma 1 so as to derive T with respect to ϵ in the following theorem.

Theorem 1. *For learning rate* $\eta_t = \frac{\beta}{t+\gamma}, \beta > \frac{1}{\mu},$ *and* $\gamma > 0$*, we have*

$$\mathbb{E}[F(\boldsymbol{w}_T) - F(\boldsymbol{w}^*)] \leq \frac{L}{2} \frac{v}{TI + \gamma}, \tag{19}$$

where v *is*

$$v = \frac{\beta^2}{\beta\mu - 1} \left\{ \sum_{k=1}^{N} \frac{\sigma_k^2}{N^2} + \frac{d}{2^{2n}}(1-\mu) + \frac{4dIG^2}{K2^{2m}} + 4(I-1)^2 G^2 + \frac{4(N-K)}{K(N-1)} I^2 G^2 \right\}. \tag{20}$$

Proof. See Appendix C. □

We can see that high precision levels for n and m can reduce the required number of communication rounds for the convergence. If we set $n = n_{\max}$ and $m = m_{\max}$, we can approximately recover the result of [22] since the quantization error decays exponentially with

respect to n and m. The convergence rate also increases with K. However, all these improvements come at the cost of consuming more energy. From Theorem 1, we bound (19) using ϵ in (18d) as follows

$$\mathbb{E}[F(\boldsymbol{w}_T) - F(\boldsymbol{w}^*)] \leq \frac{L}{2}\frac{v}{TI+\gamma} \leq \epsilon. \tag{21}$$

Now, we express each objective function as function of the control variables using Theorem 1. For notational simplicity, we use $g_1(I, K, m, n)$ for the expected total energy consumption and $g_2(I, K, m, n)$ for the number of communication rounds T. Since K devices are randomly selected according to a uniform distribution at each communication round, we can derive the expectation of the energy consumption in (18a) as follows

$$g_1(I, K, m, n) = \mathbb{E}\left[\sum_{t=1}^{T}\sum_{k\in\mathcal{N}_t} E^{UL,k}(m) + IE^{C,k}(n)\right] = \frac{KT}{N}\sum_{k=1}^{N}\left\{E^{UL,k}(m) + IE^{C,k}(n)\right\}. \tag{22}$$

Next, we derive $g_2(I, K, m, n)$ in a closed-form to fully express the objective functions and to remove the accuracy constraint (18d). For any feasible solution that satisfies (18d) with equality, we can always choose $T_0 > T$ such that T_0 still satisfies (18d). Since such T_0 will increase the value of the objectives, the accuracy constraint (18d) should be satisfied with equality [10]. Hence, we take equality in (21) to obtain:

$$\begin{aligned} g_2(I, K, m, n) &= \frac{Lv}{2I\epsilon} - \frac{\gamma}{I} \\ &= \frac{L}{2I\epsilon}\frac{\beta^2}{\beta\mu - 1}\left\{\sum_{k=1}^{N}\frac{\sigma_k^2}{N^2} + \frac{d}{2^{2n}}(1-\mu) + \frac{4dIG^2}{K2^{2m}} + 4(I-1)^2G^2 + \frac{4(N-K)}{K(N-1)}I^2G^2\right\} - \frac{\gamma}{I}. \end{aligned} \tag{23}$$

Then, we can change the original problem as below

$$\min_{I,K,m,n} \left[g_1(I, K, m, n), g_2(I, K, m, n)\right] \tag{24a}$$

$$\text{s.t.} \qquad (18b), (18c). \tag{24b}$$

Since we have two conflicting objective functions, it is infeasible to find a global optimal solution to minimize each objective function simultaneously. Hence, we consider the set of *Pareto optimal points* to obtain an efficient collection of solutions to minimize each objective function and capture the tradeoff. It is known that the set of all Pareto optimal points forms a Pareto boundary in two-dimensional space. Therefore, we use the so-called normal boundary inspection (NBI) method to obtain evenly distributed Pareto optimal points [24].

We first introduce some terminologies to facilitate the analysis. For a multi-objective function $\boldsymbol{g}(\boldsymbol{x}) = [g_1(\boldsymbol{x}), g_2(\boldsymbol{x}), \dots g_M(\boldsymbol{x})]^T$ and a feasible set $\mathcal{C}$, we define $\boldsymbol{x}_i^*$ as a global solution to minimize $g_i(\boldsymbol{x})$, $i = 1 \dots M$, over $\boldsymbol{x} \in C$. Let $\boldsymbol{g}_i^* = \boldsymbol{g}(\boldsymbol{x}_i^*)$ for $i = 1 \dots M$, and we define the utopia point $\boldsymbol{g}^*$, which is composed of individual global minima $\boldsymbol{g}_i^*$. We define the $M \times M$ matrix Φ, whose ith column is $\boldsymbol{g}_i^* - \boldsymbol{g}^*$. The set of the convex combinations of $\boldsymbol{g}_i^* - \boldsymbol{g}^*$ such that $\{\Phi\boldsymbol{\zeta} \mid \zeta_i \geq 0 \text{ and } \sum_{i=1}^{M} \zeta_i = 1\}$ is defined as convex hull of individual minima (CHIM) [24]. For simplicity, we now use $\mathcal{C}$ to represent all feasible constraint sets (18b) - (18c). We also define $\boldsymbol{x}_i^*$ as (I, K, m, n) such that $g_i(I, K, m, n)$ can be minimized over $\mathcal{C}$ for $i = 1$ and 2.

The basic premise of NBI is that any intersection points between the boundary of $\{\boldsymbol{g}(I, K, m, n) \mid (I, K, m, n) \in \mathcal{C}\}$ and a vector pointing toward the utopia point emanating from the CHIM are Pareto optimal. We can imagine that the set of Pareto optimal points will form a curve connecting $\boldsymbol{g}(\boldsymbol{x}_1^*) = [g_1(\boldsymbol{x}_1^*), g_2(\boldsymbol{x}_1^*)]$ and $\boldsymbol{g}(\boldsymbol{x}_2^*) = [g_1(\boldsymbol{x}_2^*), g_2(\boldsymbol{x}_2^*)]$. Hence, we first need to obtain $\boldsymbol{x}_1^*$ and $\boldsymbol{x}_2^*$. In the next two subsections, we will minimize $g_1(I, K, m, n)$ and $g_2(I, K, m, n)$ separately.

A. *Minimizing* $g_1(I, K, m, n)$

Since $\boldsymbol{x}_1^*$ is a global solution to minimize $g_1(I, K, m, n)$, we can find it solving:

$$\min_{I,K,m,n} \quad g_1(I, K, m, n) \tag{25a}$$

$$\text{s.t.} \quad (I, K, m, n) \in \mathcal{C}. \tag{25b}$$

This problem is non-convex because the control variables are an integer and the constraints are not a convex set. For tractability, we relax the control variables as continuous variables. The relaxed variables will be rounded back to integers for feasibility. From (22) and (23), we can see that $g_1(I, K, m, n)$ is a linear function with respect to K. Therefore, K_{min} always minimizes $g_1(I, K, m, n)$. Moreover, the relaxed problem is convex with respect to I since $\frac{\partial^2 g_1(I,K,m,n)}{\partial I^2} > 0$. Hence, we can obtain the optimal I to minimize $g_1(I, K, m, n)$ from the first derivative test as below

$$\frac{\partial g_1(I, K, m, n)}{\partial I} = H_1 I^3 + H_2 I^2 + H_3 = 0, \tag{26}$$

where

$$H_1 = 8G^2 + \frac{8(N - K_{\text{min}})G^2}{K_{\text{min}}(N-1)} \sum_{k=1}^{N} E^{C,k}(n), \tag{27}$$

$$H_2 = 8G^2\left\{\frac{d}{K_{\min}2^{2m+1}}-1\right\}\sum_{k=1}^{N}E^{C,k}(n)+4G^2\left\{\frac{(N-K_{\min})}{K_{\min}(N-1)}+1\right\}\sum_{k=1}^{N}E^{UL,k}(m), \quad (28)$$

$$H_3 = -\sum_{k=1}^{N}E^{UL,k}(m)\left\{\sum_{k=1}^{N}\frac{\sigma_k^2}{N^2}+\frac{d(1-\mu)}{2^{2n}}+4G^2-\frac{2\epsilon(\beta\mu-1)\gamma}{L\beta^2}\right\}. \quad (29)$$

Here, H_1 and H_3 express the cost of local training and the cost of transmission, respectively, while H_2 depends on both of them. We next present a closed-form solution of the above equation from Cardano's formula [25].

Lemma 2. *For given m and n, the optimal I' to minimize $g_1(I,K,m,n)$ is given by*

$$I' = \sqrt[3]{-\frac{H_2^3}{27H_1^3}-\frac{H_3}{2H_1}+\sqrt{\frac{1}{4}\left(\frac{2H_2^3}{27H_1^3}+\frac{H_3}{H_1}\right)^2+\frac{1}{27}\left(\frac{H_2^2}{3H_1^2}\right)^3}} + \sqrt[3]{-\frac{H_2^3}{27H_1^3}-\frac{H_3}{2H_1}-\sqrt{\frac{1}{4}\left(\frac{2H_2^3}{27H_1^3}+\frac{H_3}{H_1}\right)^2+\frac{1}{27}\left(\frac{H_2^2}{3H_1^2}\right)^3}}-\frac{H_2}{3H_1} \quad (30)$$

From Lemma 2, we can see that the value of I' decreases due to the increased cost of local training H_1 as we allocate a larger n. Since the quantization error decreases as n increases, a large I' is not required. Hence, an FL system can decrease the value of I' to reduce the increased local computation energy. We can also see that I' increases as the cost of transmission H_3 increases. Then, for convergence, the FL algorithm can perform more local iterations instead of frequently exchanging model parameters due to the increased communication overhead.

Although $g_1(I,K,m,n)$ is non-convex with respect to m, there exists $m' \in \mathcal{C}$ such that for $m \le m'$, $g_1(I,K,m,n)$ is non-increasing, and for $m \ge m'$, $g_1(I,K,m,n)$ is non-decreasing. This is because $g_1(I,K,m,n)$ decreases as the convergence rate becomes faster for increasing m. Then, $g_1(I,K,m,n)$ increases after m' due to unnecessarily allocated bits. Since $g_1(I,K,m,n)$ is differentiable at m, we can find such local optimal m' from $\partial g_1(I,K,m,n)/\partial m = 0$ using Fermat's Theorem [4]. To obtain m', we formulate the transcendental equation as below

$$\frac{\partial g_1(I,K,m,n)}{\partial m} = \frac{M_A}{M_B U_m}2^m + C_m = 0, \quad (31)$$

where

$$U_m = \sum_{k=1}^{N}\frac{\log 4\ p_k||\boldsymbol{d}_t^k||}{B\log_2\left(1+\frac{p_k h_k}{N_0 B}\right)m_{\max}},$$

$$M_A = \frac{K_{\min}}{N}\left\{\frac{L\beta^2}{2\epsilon I(\beta\mu-1)}\left(\frac{\sum_{k=1}^{N}\sigma_k^2}{N^2}+\frac{d(1-\mu)}{2^{2n}}+4G^2(I-1)^2+\frac{4(N-K_{\min})I^2G^2)}{K_{\min}(N-1)}\right)-\frac{\gamma}{I}\right\},$$

$$M_B = \frac{K_{\min}}{N}\frac{L\beta^2}{2\epsilon(\beta\mu-1)}\frac{4dG^2}{K_{\min}}, \text{ and } C_m = \frac{1}{\log 4} - \log 4\frac{\sum_{k=1}^{N} IE^{C,k}(n)}{U_m}. \tag{32}$$

We present a closed-form solution of the above equation in the following Lemma.

Lemma 3. *For given I and n, the local optimal m' to minimize $g_1(I,K,m,n)$ will be:*

$$m' = C_m - \frac{1}{\log 4} W\left(-\frac{M_A}{M_B U_m}\log 4 e^{C_m \log 4}\right), \tag{33}$$

where $W(\cdot)$ is the Lambert W function.

Following the same logic of obtaining m', we can find a local optimal solution n' from the first derivative test. Although there is no analytical solution for n', we can still obtain it numerically using a line search method. Then, problem (25a) can be optimized iteratively. We first obtain two analytical solutions for I and m. From these solutions, we numerically find a local optimal n'. Since $g_1(I,K,m,n)$ has a unique solution to each variable, it converges to a stationary point [26]. Although these points cannot guarantee to obtain globally Pareto optimal, using the NBI method, we are still guaranteed to reach locally Pareto optimal points [24]. In Section IV, we will also numerically show that the obtained points can still cover most of the practical portion of a global Pareto boundary. For ease of exposition, hereinafter, we refer to these local Pareto optimal points as "Pareto optimal".

B. Minimizing $g_2(I,K,m,n)$

Now, we obtain $\boldsymbol{x}_2^*$ from the following problem to complete finding the utopia point.

$$\min_{I,K,m,n} \quad g_2(I,K,m,n) \tag{34a}$$

$$\text{s.t.} \quad (I,K,m,n) \in \mathcal{C}. \tag{34b}$$

From (23), the objective function is a decreasing function with respect to K, m, and n. Hence, $N, m_{\max}$, and $n_{\max}$ are always the optimal solutions to the above problem. Then, the problem can be reduced to a single variable optimization problem with respect to I. We check the convexity of the reduced problem as follows:

$$\frac{\partial^2 g_2(I,K,m,n)}{\partial I^2} = \frac{L\beta^2}{2\epsilon(\beta\mu-1)}\left\{\sum_{k=1}^{N}\frac{2\sigma_k^2}{I^3N^2} + \frac{2d(1-\mu)}{I^3 2^{2n}} + \frac{8G^2}{I^3}\right\} - \frac{2\gamma^2}{I^3}. \tag{35}$$

Hence, it is a convex problem for $\gamma < \sqrt{\frac{L\beta^2}{2\epsilon(\beta\mu-1)}\left[\sum_{k=1}^{N}\frac{2\sigma_k^2}{N^2} + \frac{2d(1-\mu)}{2^{2n}} + 4G^2\right]}$. We present a closed-form solution of I from the first derivative test in the following lemma.

Lemma 4. *For* $\gamma < \sqrt{\frac{L\beta^2}{2\epsilon(\beta\mu-1)}[\sum_{k=1}^{N}\frac{2\sigma_k^2}{N^2}+\frac{2d(1-\mu)}{2^{2n}}+4G^2]}$*, the optimal value of* I'' *to minimize* $g_2(I,K,m,n)$ *is given by*

$$I'' = \sqrt{\frac{\sum_{k=1}^{N}\frac{\sigma_k^2}{N^2}+\frac{2d(1-\mu)}{2^{2n}}+4G^2-\frac{2\epsilon(\beta\mu-1)\gamma}{L\beta^2}}{4G^2+\frac{4(N-K)}{K(N-1)}G^2}}. \tag{36}$$

From Lemma 4, we can see that the optimal value of I'' increases as n decreases. This is because the system has to reduce quantization error by training more number of times.

C. Normal Boundary Inspection

We now obtain the Pareto boundary using NBI. We redefine $\boldsymbol{g}(I,K,m,n) := \boldsymbol{g}(I,K,m,n) - \boldsymbol{g}^*$ so that the utopia point can be located at the origin. The NBI method aims to find intersection points between the boundary of $\boldsymbol{g}(I,K,m,n)$ and a normal vector $\hat{\boldsymbol{n}} = -\boldsymbol{\Phi}\mathbf{1}$, where $\mathbf{1}$ denotes the column vector consisting of only ones which are pointing toward the origin. Then, the set of points on such a normal vector will be: $\boldsymbol{\Phi}\zeta + s\hat{\boldsymbol{n}}$, where $s \in \mathbb{R}$. The intersection points can be obtained from the following subproblem:

$$\max_{I,K,m,n,s} \quad s \tag{37a}$$

$$\text{s.t.} \quad (I,K,m,n) \in \mathcal{C} \tag{37b}$$

$$\boldsymbol{\Phi\zeta} + s\hat{\boldsymbol{n}} = \boldsymbol{g}(I,K,m,n), \tag{37c}$$

where (37c) makes the set of points on $\boldsymbol{\Phi}\zeta + s\hat{\boldsymbol{n}}$ be in the feasible area. From the definitions of $\boldsymbol{\Phi}$ and $\hat{\boldsymbol{n}}$, constraint (37c) can be given as

$$\boldsymbol{\Phi\zeta} + s\hat{\boldsymbol{n}} = \begin{bmatrix} g_1(\boldsymbol{x}_2^*)(\zeta_2 - s) \\ g_2(\boldsymbol{x}_1^*)(\zeta_1 - s) \end{bmatrix} = \begin{bmatrix} g_1(I,K,m,n) \\ g_2(I,K,m,n) \end{bmatrix}. \tag{38}$$

From (38), we obtain the expression of s as below

$$s = \zeta_1 - \frac{g_2(I,K,m,n)}{g_2(\boldsymbol{x}_1^*)} = \zeta_2 - \frac{g_1(I,K,m,n)}{g_1(\boldsymbol{x}_2^*)}. \tag{39}$$

Hence, we can change problem (37a) as follows

$$\min_{I,K,m,n} \quad \frac{g_2(I,K,m,n)}{g_2(\boldsymbol{x}_1^*)} - \zeta_1 \tag{40a}$$

$$\text{s.t.} \quad (I,K,m,n) \in \mathcal{C} \tag{40b}$$

$$1 - 2\zeta_1 + \frac{g_2(I,K,m,n)}{g_2(\boldsymbol{x}_1^*)} - \frac{g_1(I,K,m,n)}{g_1(\boldsymbol{x}_2^*)} = 0, \tag{40c}$$

where we substituted s with (39) for the objective function, constraint (40c) is from (39), and $\zeta_1+\zeta_2=1$. To remove the equality constraint (40c), we approximate the problem by introducing a quadratic penalty term λ as below

$$\min_{I,K,m,n} \quad \frac{g_2(I,K,m,n)}{g_2(\boldsymbol{x}_1^*)} - \zeta_1 + \lambda\left(1-2\zeta_1+\frac{g_2(I,K,m,n)}{g_2(\boldsymbol{x}_1^*)}-\frac{g_1(I,K,m,n)}{g_1(\boldsymbol{x}_2^*)}\right)^2 \tag{41a}$$

$$\text{s.t.} \quad (I,K,m,n)\in\mathcal{C}. \tag{41b}$$

For λ, we consider an increasing sequence $\{\lambda_i\}$ with $\lambda_i\to\infty$ as $i\to\infty$ to penalize the constraint violation more strongly. We then obtain the corresponding solution $\boldsymbol{x}^i$, which is (I,K,m,n) for minimizing problem (41a) with penalty parameter λ_i.

Theorem 2. *For $\lambda_i\to\infty$ as $i\to\infty$, solution $\boldsymbol{x}^i$ approaches the global optimal solution of problem* (41a)*, and it also becomes Pareto optimal.*

Proof. For notational simplicity, we use $\boldsymbol{x}$ to denote $(I,K,m,n)\in\mathcal{C}$. Let $q^p(\boldsymbol{x})$ denote the quadratic penalty term in problem (41a). We also define a global optimal solution to the problem (40a) as $\bar{\boldsymbol{x}}$. Since $\boldsymbol{x}^i$ minimizes the above problem with penalty parameter λ_i, we have

$$\frac{g_2(\boldsymbol{x}^i)}{g_2(\boldsymbol{x}_1^*)} - \zeta_1 + \lambda_i q^p(\boldsymbol{x}^i) \le \frac{g_2(\bar{\boldsymbol{x}})}{g_2(\boldsymbol{x}_1^*)} - \zeta_1 + \lambda_i q^p(\bar{\boldsymbol{x}}) \le \frac{g_2(\bar{\boldsymbol{x}})}{g_2(\boldsymbol{x}_1^*)} - \zeta_1, \tag{42}$$

where the last inequality is from the fact that $\bar{\boldsymbol{x}}$ minimizes problem (40a) with the equality constraint of $q^p(\bar{\boldsymbol{x}})$ being zero. Then, we obtain the inequality of $q^p(\boldsymbol{x}^i)$ as follows

$$q^p(\boldsymbol{x}^i) \le \frac{1}{\lambda_i}\left(\frac{g_2(\bar{\boldsymbol{x}})}{g_2(\boldsymbol{x}_1^*)} - \frac{g_2(\boldsymbol{x}^i)}{g_2(\boldsymbol{x}_1^*)}\right). \tag{43}$$

By taking the limit as $i\to\infty$, we have

$$\lim_{i\to\infty} q^p(\boldsymbol{x}^i) \le \lim_{i\to\infty}\frac{1}{\lambda_i}\left(\frac{g_2(\bar{\boldsymbol{x}})}{g_2(\boldsymbol{x}_1^*)} - \frac{g_2(\boldsymbol{x}^i)}{g_2(\boldsymbol{x}_1^*)}\right) = 0. \tag{44}$$

Hence, as $\lambda_i\to\infty$, we can see that $\boldsymbol{x}^i$ approaches the global optimal solution of (40a), which aims to find a Pareto optimal point. □

From Theorem 2, we now have a Pareto optimal point of problem (18a) for specific values of ζ_1 and ζ_2. Note that problem (41a) can be solved using a software solver. To fully visualize the boundary, we iterate problem (37a) for various combinations of ζ_1 and ζ_2. The overall algorithm is given in Algorithm 2.

Algorithm 2: NBI approach to obtain Pareto boundary

Input: $N, B, p, I_{\min}, K_{\min}, m_{\max}, n_{\max}, \beta, \gamma, G, \sigma, \mu, L, A, \alpha$, accuracy constraint ϵ, loss function $F_k(\cdot)$, stopping criterion Γ_1 and Γ_2, and a structure of QNN

To find $\boldsymbol{g}_1^*$, initialize (I, K, m, n) and set $K = N$
while $\sqrt{(I-I')^2 + (m-m')^2 + (n-n')^2} > \Gamma_1$ **do**
    Update (I, m, n) as (I', m', n')
    Obtain I' from (30)
    Obtain m' for fixed I' from (33)
    Obtain n' for fixed I' and m' using a line search
To find $\boldsymbol{g}_2^*$, calculate I'' from Lemma 4 and set $(K, m, n) = (N, m_{\max}, n_{\max})$
while $\zeta_1 \leq 1$ **do**
    Initialize $\boldsymbol{x}$, which denotes a vector (I, K, m, n) **repeat**
        Update $\boldsymbol{x}$ as $\boldsymbol{x}'$
        Obtain $\boldsymbol{x}'$ from problem (41a)
        Increase λ
    until $\sqrt{||\boldsymbol{x} - \boldsymbol{x}'||^2} \leq \Gamma_2$;
    Increase ζ_1

D. Nash Bargaining Solution

Since the solutions from (18a) are Pareto optimal, there is always an issue of choosing the best point. This is because any improvement on one objective function leads to the degradation of another. We can tackle this problem considering a bargaining process [27] between two players: one tries to minimize the energy consumption and another aims to reduce the number of communication rounds. Since the parameters of FL, i.e., (I, K, m, n), are shared, the players should reach a certain agreement over the parameters. It is known that NBS can be a unique solution to this bargaining process, and it can be obtained from the following problem [27]:

$$\max_{g_1(\boldsymbol{x}), g_2(\boldsymbol{x})} \quad (g_1(\boldsymbol{D}) - g_1(\boldsymbol{x}))(g_2(\boldsymbol{D}) - g_2(\boldsymbol{x})) \tag{45a}$$

$$\text{s.t.} \quad (g_1(\boldsymbol{x}), g_2(\boldsymbol{x})) \in \overline{g_{\text{ach}}}, \tag{45b}$$

where $g_{\text{ach}} = \bigcup_{\boldsymbol{x} \in \mathcal{C}} (g_1(\boldsymbol{x}), g_2(\boldsymbol{x}))$ is the achievable set of $(g_1(\boldsymbol{x}), g_2(\boldsymbol{x}))$, $\overline{g_{\text{ach}}}$ represents the convex hull of g_{ach}, and $\boldsymbol{D}$ is the outcome when the players fail to cooperate. Since the NBS always lies on the Pareto boundary, we perform the bargaining process on the obtained boundary from Algorithm 2. Then, we can find the NBS graphically by finding a tangential point where the boundary and a parabola $(g_1(\boldsymbol{D}) - g_1(\boldsymbol{x}))(g_2(\boldsymbol{D}) - g_2(\boldsymbol{x}) = \Delta$ intersects with constant Δ.

IV. Simulation Results and Analysis

For our simulations, unless stated otherwise, we uniformly deploy $N = 50$ devices over a square area of size 500 m $\times$ 500 m serviced by one BS at the center, and we assume a Rayleigh fading channel with a path loss exponent of 4. We assume that the FL algorithm is used for a classification task with MNIST data set. A softmax classifier is used to measure our FL performance. We also use $P = 100$ mW, $B = 10$ MHz, $N_0 = -173$ dBm, $m_{\text{max}} = 32$ bits, $n_{\text{max}} = 32$ bits, $I_{\text{min}} = 1$, $I_{\text{max}} = 50$, $K_{\text{min}} = 1$, $L = 0.097$, $\mu = 0.05$, $\epsilon = 0.01$, $\gamma = 1$, and $\beta = 2/\mu$, $\forall k = 1, \ldots, N$ [28]–[30]. We assume that each device trains a QNN structure with five convolutional layers and three fully-connected layers. Specifically, the convolutional layers consist of 128 kernels of size 3 × 3, two of 64 kernels of size 3×3, and two of 32 kernels of size 3x3. The first layer is followed by 3x3 pooling and the second and the fifth layer are followed by 3x3 max pooling with a stride of two. Then, we have one dense layer of 2000 neurons, one fully-connected layer of 100 neurons, and the output layer. In this setting, we have $N_c = 0.0405 \times 10^9, N_s = 0.416 \times 10^6$, and $O_s = 4990$. To estimate G and σ_k, we measure every user's average maximum norm of stochastic gradients G_k for the initial 20 iterations and set $G = \max_k \ G_k$, $\forall k = \{1, \ldots, N\}$. Since the norm of the stochastic gradient generally decreases with the training epochs, we use the initial values of G_k to estimate G as in [31] and [32]. From the above setting, we estimated $G = 0.05$ and used it to bound σ_k. For the computing model, we use a 28 nm technology processing chip and set $A = 3.7$ pJ and $\alpha = 1.25$ as done in [20]. For the disagreement point $\boldsymbol{D}$, we use $(I_{\text{max}}, N/2, 1, 1)$ as this setting is neither biased towards minimizing the energy consumption nor towards the number of communication rounds. We assume that each device has the same architecture of the processing chip. All statistical results are averaged over $10,000$ independent runs

Figure 3 shows the Pareto boundary from Algorithm 2 as well as the feasible area obtained from the exhaustive search for $N = 50$. We can see that our boundary and the actual Pareto boundary match well. Although we cannot find the global Pareto optimal points due to the non-convexity of problem (25a), it is clear that our analysis can still cover most of the important points that can effectively show the tradeoff in the feasible region.

Figure 4 and Table I show the Pareto boundaries obtained from the NBI method and the solutions of four possible operating points, respectively, for varying N. SUM represents the point that minimizes the sum of the two objectives. E_{min} and T_{min} are the solutions that separately

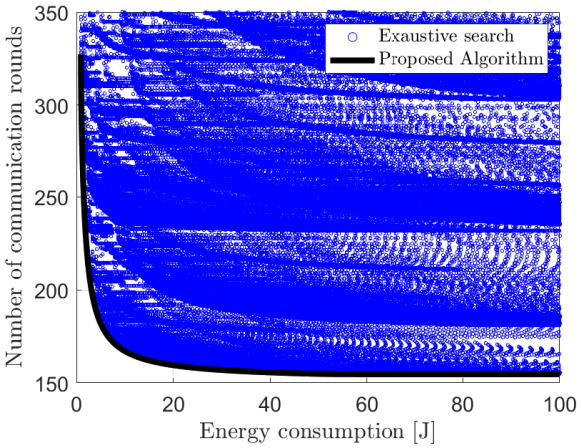

Fig. 3: Pareto Boundary from Algorithm 2 and feasible area from exhaustive search

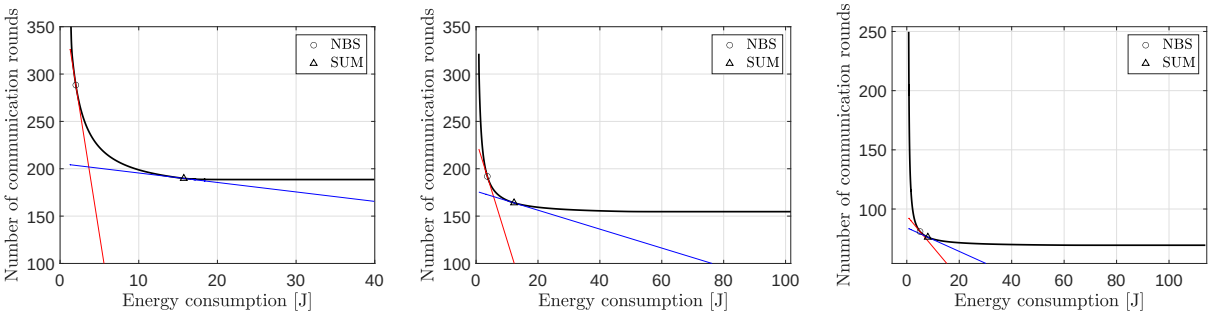

(a) N = 10 (b) N = 50 (c) N = 200

Fig. 4: Pareto boundaries, NBS, and SUM points for varying the number of devices N.

	$N = 10$	$N = 50$	$N = 200$
NBS	$(2, 3, 12, 14)$	$(2, 4, 13, 15)$	$(1, 17, 13, 16)$
SUM	$(3, 9, 13, 15)$	$(2, 13, 13, 16)$	$(1, 28.13.16)$
E_{min}	$(2, 1, 11, 13)$	$(1, 1, 12, 14)$	$(1, 1, 12, 14)$
T_{min}	$(3, 10, 32, 32)$	$(2, 50, 32, 32)$	$(1, 200, 32, 32)$

TABLE I: Corresponding solutions of NBS, SUM, E_{min}, and T_{min} for varying N.

optimize $g_1(I, K, m, n)$ and $g_2(I, K, m, n)$, respectively. From Fig. 4, we can see that the energy consumption increases while the number of communication rounds decreases to achieve the target accuracy for increasing N. The FL system can choose more devices at each communication round as N increases. Hence, the impact of SG variance decreases as shown in Theorem 1. Since involving more devices in the averaging process implies an increase in the size of the batch, the convergence rate increases by using more energy [33].

From Table I and Fig. 4, we can see that NBS points are more biased toward reducing the

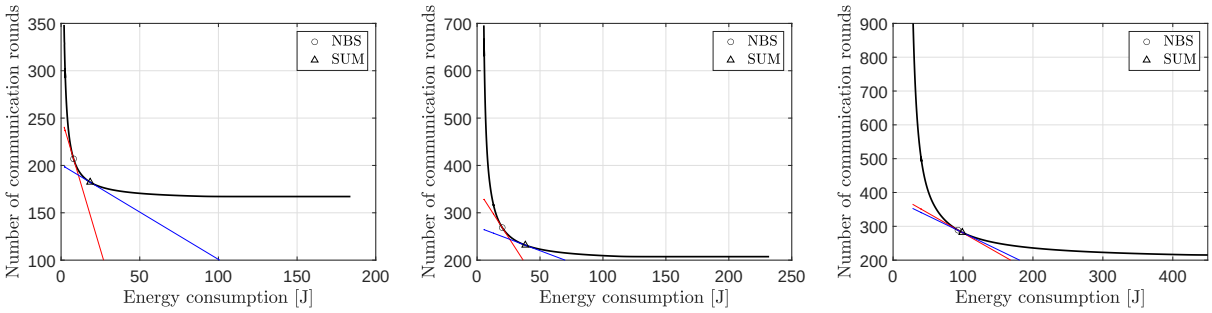

(a) CNN model 1 (b) CNN model 2 (c) CNN model 3

Fig. 5: Pareto boundaries, NBS, and SUM points for varying the size of neural networks.

	CNN1	CNN2	CNN3
NBS	$(2, 5, 13, 15)$	$(1, 8, 14, 16)$	$(1, 19, 14, 17)$
SUM	$(2, 11, 13, 16)$	$(1, 17, 14, 16)$	$(1, 10, 14, 17)$
E_{min}	$(2, 1, 12, 14)$	$(1, 1, 13, 15)$	$(1, 1, 14, 15)$
T_{min}	$(2, 50, 32, 32)$	$(1, 50, 32, 32)$	$(1, 50, 32, 32)$

TABLE II: Corresponding solutions of NBS, SUM, E_{min}, and T_{min} for varying the size of neural networks.

energy consumption while the SUM points focus on minimizing communication rounds. We can also see that, as N becomes larger, the optimal I decreases while the other variables increase. This is because I is a decreasing function with respect to G as shown in Lemmas 2 and 4. Hence, the FL system decreases I to avoid model discrepancy over devices since the estimated value of G becomes larger for increasing N. However, a small I will slow down the process to reach optimal weights in the local training. To mitigate this, the FL system then increases (K, m, n) so that it can obtain more information in the averaging process by selecting more devices and reducing the quantization error.

Figure 5 and Table II present the Pareto boundaries and the corresponding solutions when increasing the size of the neural networks. We keep the same structure of our default CNN, but we now increase the number of neurons in the convolutional layers. For each CNN model, the number of parameters will be 0.55×10^6, 1.61×10^6, and 5.6×10^6, respectively. Fig. 5 and Table II show that the energy consumption and the number of communication rounds until convergence increase with the size of neural networks. From Table II, we can see that the FL system requires higher precision levels and needs to select more devices at each communication round for larger neural networks. This is because the quantization error increases for larger neural networks, as

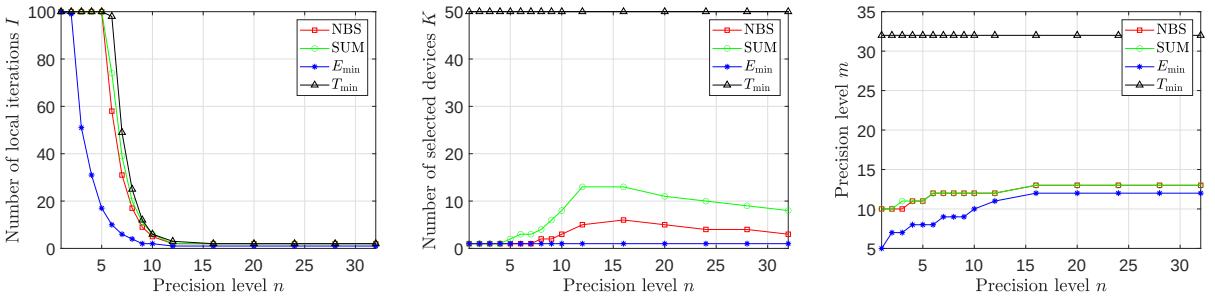

(a) Impact of increasing n on I (b) Impact of increasing n on K (c) Impact of increasing n on m

Fig. 6: Impact of increasing precision level n on (I, K, m).

per Lemma 1. Hence, the FL system selects more devices and allocates more bits for both the computation and the transmission so as to mitigate the quantization error. This, in turn, means that the use of larger neural networks will naturally require more energy, even if the neural network is quantized.

Figure 6 presents the optimal (I, K, m) for fixed values of n when $I_{\max} = 100$. In Fig. 6a, we can see that the optimal I decreases as n increases. When n is small, the devices must perform many iterations in order to reduce the quantization error from the low precision. As n increases, the quantization error decreases exponentially as per Lemma 1, and thus, the optimal I decreases accordingly. From Fig. 6b, we also observe that K increases and then decreases with n. This is because the FL system chooses to obtain more information by increasing K in the averaging process to mitigate the quantization error from a low precision n. However, K decreases after a certain n to save the energy since local training becomes expensive. Similarly, in Fig. 6c, we can see that the FL system allocates more precision in the transmission so that it can enhance the convergence rate. Unlike K, the precision level m does not decrease after a certain n. This is because the FL system must keep sufficient precision during transmission so that it can maintain a reasonable convergence rate when decreasing K shown in Fig. 6b.

In Fig. 7, we show the performance of the NBS and the SUM points with increasing K. We can see that the required communication rounds decrease as K increases for both schemes. Hence, we can improve the convergence rate by increasing K at the expense of more energy. This corroborates the analysis in Section III-A, which shows the total energy consumption is linear with respect to K. Similarly, it also corroborates the fact that the required number of communication rounds to achieve a certain ϵ is a decreasing function of K in Section III-B.

Figure 8 compares the performance of the proposed model with the three baselines for varying

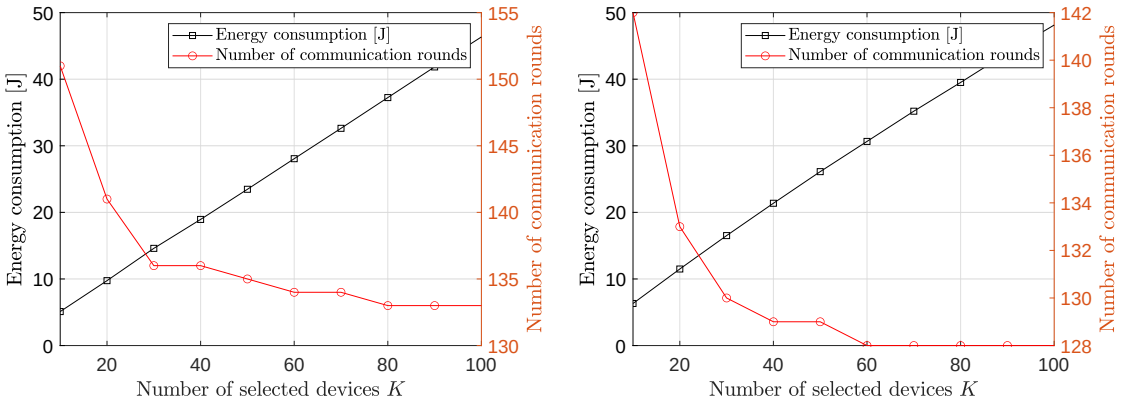

(a) Performance of NBS with different K

(b) Performance of SUM with different K

Fig. 7: Performance of NBS and SUM points for increasing K.

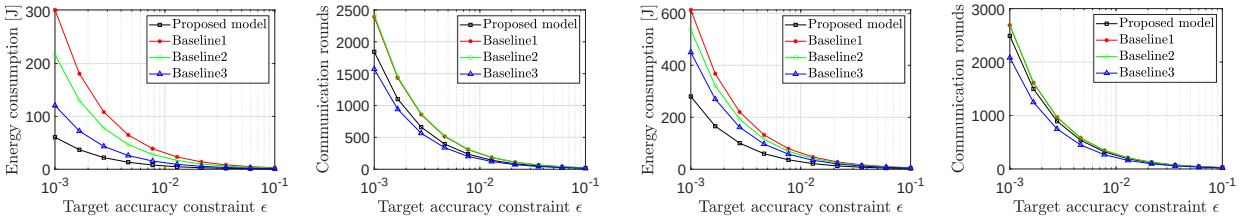

(a) Performance of the proposed model and the baselines to achieve ϵ using the default CNN

(b) Performance of the proposed model and the baselines to achieve ϵ using CNN model 2

Fig. 8: Comparison of the performance between the proposed model and the baselines to achieve target accuracy ϵ.

ϵ using the NBS points. We used two CNN models, which are the default CNN structure and the second CNN structure from Figs. 5. Baseline 1 uses $(1, 10, 32, 32)$, Baseline 2 only optimizes m and uses the same setting as Baseline 1, and Baseline 3 optimizes (I, K) while data are represented in full-precision [10]. From Fig. 8a and 8b, we can see that our model can reduce the energy consumption significantly compared with the baselines, especially when high accuracy is required. However, we can observe that Baseline 3 achieves a better convergence rate since it allocates full-precision for the computation and the transmission at more expense of energy. From Baseline 1 and Baseline 2, we observe that quantization during transmission is beneficial to save the energy, and it does not significantly affect the convergence rate. In particular, for CNN model 2, we can achieve around 52% of energy savings compared to Baseline 1 while the number of communication rounds will increase by only 19% compared to that of Baseline 3.

V. Conclusion

In this paper, we have studied the problem of energy-efficient quantized FL over wireless networks. We have presented the energy model for our FL based on the physical structure of a processing chip considering the quantization. Then, we have formulated a multi-objective optimization problem to minimize the energy consumption and the number of communication rounds simultaneously under a certain target accuracy by controlling the number of local iterations, the number of selected users, the precision levels for the transmission, and the computation. To solve this problem, we first have derived the convergence rate of our quantized FL. Based on it, we have used the NBI method to obtain the Pareto boundary. We also have derived analytical solutions that can optimize each objective function separately. Simulation results have validated our theoretical analysis and provided design insights with two practical operating points. We have also shown that our model requires much less energy than a standard FL model and the baselines to achieve the convergence. In essence, this work provides the first systematic study of how to optimally design quantized FL balancing the tradeoff between energy efficiency and convergence rate over wireless networks.

Appendix

A. Additional Notations

As done in [22], we define t as the round of the local iteration with a slight abuse of notation. Then, $\boldsymbol{w}_t^k$ becomes the model parameter at local iteration t of device k. If $t \in \mathcal{I}$, where $\mathcal{I} = \{jI \mid j = 1, 2, \dots\}$, each device transmits model update $\boldsymbol{d}_t^{Q,k}$ to the BS. We introduce an auxiliary variable $\boldsymbol{v}_{t+1}^k$ to represent the result of one step of local training from $\boldsymbol{w}_t^k$. At each local training, device k updates its local model using SGD as below

$$\boldsymbol{v}_{t+1}^k = \boldsymbol{w}_t^k - \eta_t \nabla F_k(\boldsymbol{w}_t^{Q,k}, \xi_t^k). \tag{46}$$

The result of the $(t+1)$th local training will be $\boldsymbol{w}_{t+1}^k = \boldsymbol{v}_{t+1}^k$ if $t+1 \notin \mathcal{I}$ because device k does not send a model update to the BS. If $t+1 \in \mathcal{I}$, each device calculates and transmits its model update, and then the global model is generated as $\boldsymbol{w}_{t+1} = \boldsymbol{w}_{t-I+1} + \frac{1}{K}\sum_{k\in\mathcal{N}_{t+1}} \boldsymbol{d}_{t+1}^{Q,k}$. Note that $\boldsymbol{d}_{t+1}^{Q,k} = Q(\boldsymbol{v}_{t+1}^k - \boldsymbol{w}_{t-I+1})$ and $\boldsymbol{w}_{t-I+1}$ is the most recent global model received from the BS. We provide the aforementioned cases below:

$$\boldsymbol{w}_{t+1}^k = \begin{cases} \boldsymbol{v}_{t+1}^k & \text{if} \quad t+1 \notin \mathcal{I}, \\ \boldsymbol{w}_{t-I+1} + \frac{1}{K}\sum_{k\in\mathcal{N}_{t+1}} \boldsymbol{d}_{t+1}^{Q,k} & \text{if} \quad t+1 \in \mathcal{I}. \end{cases} \tag{47}$$

Now, we define two more auxiliary variables: $\bar{\boldsymbol{v}}_t = \frac{1}{N}\sum_{k=1}^{N} \boldsymbol{v}_t^k$ and $\bar{\boldsymbol{w}}_t = \frac{1}{N}\sum_{k=1}^{N} \boldsymbol{w}_t^k$. Similarly, we denote $\rho_t = \frac{1}{N}\sum_{k=1}^{N} \nabla F_k(\boldsymbol{w}_t^{Q,k}, \xi_t^k)$ and $\bar{\rho}_t = \frac{1}{N}\sum_{k=1}^{N} \nabla F_k(\boldsymbol{w}_t^{Q,k})$. From (46), we can see that $\bar{\boldsymbol{v}}_{t+1} = \bar{\boldsymbol{w}}_t - \eta_t \rho_t$.

B. The result of one local iteration

We present a preliminary lemma to prove Theorem 1. We first present the result of one iteration of local training in the following lemma.

Lemma 5. *Under Assumption 1, we have*

$$\mathbb{E}\left[||\bar{\boldsymbol{v}}_{t+1} - \boldsymbol{w}^*||^2\right] \leq (1-\mu\eta_t)\mathbb{E}\left[||\bar{\boldsymbol{w}}_t - \boldsymbol{w}^*||^2\right] + \frac{\eta_t^2}{N^2}\sum_{k=1}^{N}\sigma_k^2 - \frac{\mu\eta_t d}{2^{2n}} + \frac{\eta_t^2 d}{2^{2n}} + 4\eta_t^2(I-1)^2G^2. \quad (48)$$

Proof. From $\bar{\boldsymbol{v}}_{t+1} = \bar{\boldsymbol{w}}_t - \eta_t\rho_t$, we have

$$\begin{aligned} ||\bar{\boldsymbol{w}}_{t+1} - \boldsymbol{w}^*||^2 &= ||\bar{\boldsymbol{w}}_t - \eta_t\rho_t - \boldsymbol{w}^* - \eta_t\bar{\rho}_t + \eta_t\bar{\rho}_t||^2 \\ &= \underbrace{||\bar{\boldsymbol{w}}_t - \boldsymbol{w}^* - \eta_t\bar{\rho}_t||^2}_{A_1} + 2\eta_t \underbrace{\langle \bar{\boldsymbol{w}}_t - \boldsymbol{w}^* - \eta_t\bar{\rho}_t, \bar{\rho}_t - \rho\rangle}_{A_2} + \underbrace{\eta_t^2||\rho_t - \bar{\rho}_t||^2}_{A_3}. \end{aligned} \quad (49)$$

Since $\mathbb{E}[\rho_t] = \bar{\rho}$, we can know that A_2 becomes zero after taking expectation. For A_1, we split it into the three terms as below:

$$A_1 = ||\bar{\boldsymbol{w}}_t - \boldsymbol{w}^* - \eta_t\bar{\rho}_t||^2 = ||\bar{\boldsymbol{w}}_t - \boldsymbol{w}^*||^2 \underbrace{-2\eta_t\langle \bar{\boldsymbol{w}}_t - \boldsymbol{w}^*, \bar{\rho}_t\rangle}_{B_1} + \underbrace{\eta_t^2||\bar{\rho}_t||^2}_{B_2}. \quad (50)$$

We now derive an upper bound of B_1. From the definition of $\bar{\boldsymbol{w}}_t$ and $\bar{\rho}_t$, we express B_1 as

$$\begin{aligned} B_1 &= -2\eta_t\langle \bar{\boldsymbol{w}}_t - \boldsymbol{w}^*, \bar{\rho}_t\rangle = -2\eta_t\frac{1}{N}\sum_{k=1}^{N}\langle \bar{\boldsymbol{w}}_t - \boldsymbol{w}^*, \nabla F_k(\boldsymbol{w}_t^{Q,k})\rangle \\ &= -2\eta_t\frac{1}{N}\sum_{k=1}^{N}\langle \bar{\boldsymbol{w}}_t - \boldsymbol{w}_t^{Q,k}, \nabla F_k(\boldsymbol{w}_t^{Q,k})\rangle - 2\eta_t\frac{1}{N}\sum_{k=1}^{N}\langle \boldsymbol{w}_t^{Q,k} - \boldsymbol{w}^*, \nabla F_k(\boldsymbol{w}_t^{Q,k})\rangle. \end{aligned} \quad (51)$$

We first derive an upper bound of $-\langle \bar{\boldsymbol{w}}_t - \boldsymbol{w}_t^{Q,k}, \nabla F_k(\boldsymbol{w}_t^{Q,k})\rangle$ using the Cauchy-Schwarz inequality and arithmetic mean and geometric mean inequality as below

$$\begin{aligned} -\langle \bar{\boldsymbol{w}}_t - \boldsymbol{w}_t^{Q,k}, \nabla F_k(\boldsymbol{w}_t^{Q,k})\rangle &\leq \eta_t||\boldsymbol{w}_t^{Q,k} - \bar{\boldsymbol{w}}_t||\frac{1}{\eta_t}||\nabla F_k(\boldsymbol{w}_t^{Q,k})|| \\ &\leq \frac{\eta_t}{2}||\boldsymbol{w}_t^{Q,k} - \bar{\boldsymbol{w}}_t||^2 + \frac{1}{2\eta_t}||\nabla F_k(\boldsymbol{w}_t^{Q,k})||^2. \end{aligned} \quad (52)$$

We use the assumption of μ-convexity of the loss function to derive an upper bound of $-\langle \boldsymbol{w}_t^{Q,k} - \boldsymbol{w}^*, \nabla F_k(\boldsymbol{w}_t^{Q,k})\rangle$. From the fact that $F_k(\boldsymbol{w}^*) \geq F_k(\boldsymbol{w}_t^{Q,k}) + \langle \boldsymbol{w}^* - \boldsymbol{w}_t^{Q,k}, \nabla F_k(\boldsymbol{w}_t^{Q,k})\rangle + \frac{\mu}{2}||\boldsymbol{w}^* - \boldsymbol{w}_t^{Q,k}||^2$, we have

$$-\langle \boldsymbol{w}_t^{Q,k} - \boldsymbol{w}^*, \nabla F_k(\boldsymbol{w}_t^{Q,k})\rangle \leq -\{F_k(\boldsymbol{w}_t^{Q,k}) - F_k(\boldsymbol{w}^*)\} - \frac{\mu}{2}||\boldsymbol{w}^* - \boldsymbol{w}_t^{Q,k}||^2. \tag{53}$$

For B_2, we use L-smoothness of the loss function to obtain the upper bound as below

$$B_2 = \eta_t^2||\bar{\rho}_t||^2 \leq \eta_t^2 \frac{1}{N}\sum_{k=1}^{N}||\nabla F_k(\boldsymbol{w}_t^{Q,k})||^2 \leq \frac{2L\eta_t^2}{N}\sum_{k=1}^{N}(F_k(\boldsymbol{w}_t^{Q,k}) - F_k^*). \tag{54}$$

Then, we obtain an upper bound of A_1 using (52), (53), and (54) as follows

$$\begin{aligned}
A_1 \leq\ & ||\bar{\boldsymbol{w}}_t - \boldsymbol{w}^*||^2 + \frac{2L\eta_t^2}{N}\sum_{k=1}^{N}\left\{F_k(\boldsymbol{w}^{Q,k}) - F_k^*\right\} + \frac{1}{N}\sum_{k=1}^{N}\left\{\eta_t^2||\bar{\boldsymbol{w}}_t - \boldsymbol{w}_t^{Q,k}||^2 + ||\nabla F_k(\boldsymbol{w}_t^{Q,k})||^2\right\} \\
& - \frac{2\eta_t}{N}\sum_{k=1}^{N}\left\{F_k(\boldsymbol{w}_t^{Q,k}) - F_k(\boldsymbol{w}^*) + \frac{\mu}{2}||\boldsymbol{w}^* - \boldsymbol{w}_t^{Q,k}||^2\right\} \\
=\ & ||\bar{\boldsymbol{w}}_t - \boldsymbol{w}^*||^2 - \frac{\mu\eta_t}{N}\sum_{k=1}^{N}||\boldsymbol{w}_t^{Q,k} - \boldsymbol{w}^*||^2 + \frac{\eta_t^2}{N}\sum_{k=1}^{N}||\boldsymbol{w}_t^{Q,k} - \bar{\boldsymbol{w}}_t||^2 + \frac{1}{N}\sum_{k=1}^{N}||\nabla F_k(\boldsymbol{w}_t^{Q,k})||^2 \\
& - \frac{2\eta_t}{N}\sum_{k=1}^{N}\left\{F_k(\boldsymbol{w}_t^{Q,k}) - F_k(\boldsymbol{w}^*)\right\} + \frac{2L\eta_t^2}{N}\sum_{k=1}^{N}\left\{F_k(\boldsymbol{w}_t^{Q,k}) - F_k^*\right\} \\
\leq\ & ||\bar{\boldsymbol{w}}_t - \boldsymbol{w}^*||^2 - \frac{\mu\eta_t}{N}\sum_{k=1}^{N}||\boldsymbol{w}_t^{Q,k} - \boldsymbol{w}^*||^2 + \frac{\eta_t^2}{N}\sum_{k=1}^{N}||\boldsymbol{w}_t^{Q,k} - \bar{\boldsymbol{w}}_t||^2 + \underbrace{\frac{2L(\eta_t^2+1)}{N}\sum_{k=1}^{N}\left\{F_k(\boldsymbol{w}_t^{Q,k}) - F_k^*\right\}}_{C} \\
& \underbrace{- \frac{2\eta_t}{N}\sum_{k=1}^{N}\left\{F_k(\boldsymbol{w}_t^{Q,k}) - F_k(\boldsymbol{w}^*)\right\}}_{C},
\end{aligned} \tag{55}$$

where the last inequality is from L-smoothness of the loss function using $||\nabla F_k(\boldsymbol{w}_t^{Q,k})||^2 \leq 2L(F_k(\boldsymbol{w}_t^{Q,k}) - F_k^*)$. Note that F_k^* is the minimum value of F_k. For $L < \frac{\eta_t}{\eta_t^2+1}$, we can derive the upper bound of C as follows

$$\begin{aligned}
C &\leq \frac{2L(\eta_t^2+1)}{N}\sum_{k=1}^{N}\left\{F_k(\boldsymbol{w}_t^{Q,k}) - F_k^* - F_k(\boldsymbol{w}_t^{Q,k}) + F_k(\boldsymbol{w}^*)\right\} \\
&= \frac{2L(\eta_t^2+1)}{N}\sum_{k=1}^{N}\{F_k(\boldsymbol{w}^*) - F_k^*\} = 0,
\end{aligned} \tag{56}$$

where the last equation is from the independent and identically distributed (i.i.d.) assumption over the local dataset. Then, A_1 can be upper bounded as below

$$A_1 \leq ||\bar{\boldsymbol{w}}_t - \boldsymbol{w}^*||^2 - \frac{\mu\eta_t}{N}\sum_{k=1}^{N}||\boldsymbol{w}_t^{Q,k} - \boldsymbol{w}^*||^2 + \frac{\eta_t^2}{N}\sum_{k=1}^{N}||\boldsymbol{w}_t^{Q,k} - \bar{\boldsymbol{w}}_t||^2 \tag{57}$$

Now we derive $||\boldsymbol{w}_t^{Q,k} - \boldsymbol{w}^*||^2$ in A_1 as follows

$$\begin{aligned}||\boldsymbol{w}_t^{Q,k} - \boldsymbol{w}^*||^2 &= ||\boldsymbol{w}_t^{Q,k} - \boldsymbol{w}_t^k + \boldsymbol{w}_t^k - \boldsymbol{w}^*||^2 \\ &= ||\boldsymbol{w}_t^{Q,k} - \boldsymbol{w}_t||^2 + ||\boldsymbol{w}_t^k - \boldsymbol{w}^*||^2 + 2\langle \boldsymbol{w}_t^{Q,k} - \boldsymbol{w}_t^k, \boldsymbol{w}_t^k - \boldsymbol{w}^*\rangle. \end{aligned}\tag{58}$$

Note that $\langle \boldsymbol{w}_t^{Q,k} - \boldsymbol{w}_t^k, \boldsymbol{w}_t^k - \boldsymbol{w}^*\rangle$ becomes zero after taking expectation due to Lemma 1. Then, we can bound A_1 as follows

$$A_1 \leq (1-\mu\eta_t)||\bar{\boldsymbol{w}}_t - \boldsymbol{w}^*||^2 - \frac{\mu\eta_t}{N}\sum_{k=1}^{N}||\boldsymbol{w}_t^{Q,k} - \boldsymbol{w}_t^k||^2 + \frac{\eta_t^2}{N}\sum_{k=1}^{N}||\boldsymbol{w}_t^{Q,k} - \bar{\boldsymbol{w}}_t||^2 \tag{59}$$

Now we obtain the expectation of (49) using (59) as follows

$$\begin{aligned}\mathbb{E}\left[||\bar{\boldsymbol{v}}_{t+1} - \boldsymbol{w}^*||^2\right] \leq (1-\mu\eta_t)\mathbb{E}\left[||\bar{\boldsymbol{w}}_t - \boldsymbol{w}^*||^2\right] + \eta_t^2\mathbb{E}\left[||\rho_t - \bar{\rho}_t||^2\right] - \frac{\mu\eta_t}{N}\sum_{k=1}^{N}\mathbb{E}\left[||\boldsymbol{w}_t^{Q,k} - \boldsymbol{w}_t^k||^2\right] \\ + \frac{\eta_t^2}{N}\sum_{k=1}^{N}\mathbb{E}\left[||\bar{\boldsymbol{w}}_t - \boldsymbol{w}_t^{Q,k}||^2\right]\end{aligned}\tag{60}$$

To further bound (60), we express $\mathbb{E}[||\rho_t - \bar{\rho}_t||^2]$ as

$$\begin{aligned}\mathbb{E}\left[||\rho_t - \bar{\rho}_t||^2\right] &= \mathbb{E}\left[\left|\left|\frac{1}{N}\sum_{k=1}^{N}\nabla F_k(\boldsymbol{w}_t^{Q,k}, \xi_t^k) - \nabla F_k(\boldsymbol{w}_t^{Q,k})\right|\right|^2\right] \\ &= \frac{1}{N^2}\sum_{k=1}^{N}\mathbb{E}\left[\left|\left|\nabla F_k(\boldsymbol{w}_t^{Q,k}, \xi_t^k) - \nabla F_k(\boldsymbol{w}_t^{Q,k})\right|\right|^2\right] \leq \frac{1}{N^2}\sum_{k=1}^{N}\sigma_k^2,\end{aligned}\tag{61}$$

where (61) is from $\mathbb{E}[\nabla F_k(\boldsymbol{w}_t^{Q,k}, \xi_t^k)] = \nabla F_k(\boldsymbol{w}_t^{Q,k})$ and the last inequality is from Assumption 1. We also derive the upper bound of $\mathbb{E}\left[||\bar{\boldsymbol{w}}_t - \boldsymbol{w}_t^{Q,k}||^2\right]$ as below

$$\begin{aligned}\mathbb{E}\left[||\bar{\boldsymbol{w}}_t - \boldsymbol{w}_t^{Q,k}||^2\right] &= \mathbb{E}\left[||\boldsymbol{w}_t^k - \boldsymbol{w}_t^{Q,k}||^2 + ||\bar{\boldsymbol{w}}_t - \boldsymbol{w}_t^k||^2 + 2\langle \boldsymbol{w}_t^k - \boldsymbol{w}_t^{Q,k}, \bar{\boldsymbol{w}}_t - \boldsymbol{w}_t^k\rangle\right] \\ &\leq \mathbb{E}\left[||\boldsymbol{w}_t^k - \boldsymbol{w}_t^{Q,k}||^2\right] + 4\eta_t^2(I-1)^2G^2,\end{aligned}\tag{62}$$

where the last inequality is from Lemma 1 and the result of [22] for $\eta_t \leq 2\eta_{t+I}$ using

$$\frac{1}{N}\sum_{k=1}^{N}\mathbb{E}\left[||\bar{\boldsymbol{w}}_t - \boldsymbol{w}_t^k||^2\right] \leq 4\eta_t^2(I-1)^2G^2. \tag{63}$$

Then, we can obtain Lemma 5 from using (5) in Lemma 1. □

C. Proof of Theorem 1

Since we use quantization in both local training and transmission, we cannot directly use the result of [22] to derive the convergence rate due to the quantization errors. We first define an additional auxiliary variable as done in [12] to prove Theorem 1 as below

$$\boldsymbol{u}_{t+1}^k = \begin{cases} \boldsymbol{v}_{t+1}^k & \text{if} \quad t+1 \notin \mathcal{I}, \\ \frac{1}{K}\sum_{k\in\mathcal{N}_{t+1}} \boldsymbol{v}_{t+1}^k & \text{if} \quad t+1 \in \mathcal{I}. \end{cases} \tag{64}$$

We also define $\bar{\boldsymbol{u}}_t = \frac{1}{N}\sum_{k=1}^N \boldsymbol{u}_t^k$ for convenience. Since we are interested in the result of global iterations, we focus on $t+1 \in \mathcal{I}$. Then, we have

$$\begin{aligned} ||\bar{\boldsymbol{w}}_{t+1} - \boldsymbol{w}^*||^2 &= ||\bar{\boldsymbol{w}}_{t+1} - \bar{\boldsymbol{u}}_{t+1} + \bar{\boldsymbol{u}}_{t+1} + \boldsymbol{w}^*||^2 \\ &= \underbrace{||\bar{\boldsymbol{w}}_{t+1} - \bar{\boldsymbol{u}}_{t+1}||^2}_{D_1} + \underbrace{||\bar{\boldsymbol{u}}_{t+1} - \boldsymbol{w}^*||^2}_{D_2} + \underbrace{2\langle \bar{\boldsymbol{w}}_{t+1} - \bar{\boldsymbol{u}}_{t+1}, \bar{\boldsymbol{u}}_{t+1} - \boldsymbol{w}^* \rangle}_{D_3}. \end{aligned} \tag{65}$$

To simplify (65), we adopt the result of $\bar{\boldsymbol{w}}_{t+1}$ and $\bar{\boldsymbol{u}}_{t+1}$ from [12] as follows:

$$\mathbb{E}[\bar{\boldsymbol{w}}_{t+1}] = \bar{\boldsymbol{u}}_{t+1}, \tag{66}$$

$$\mathbb{E}\left[||\bar{\boldsymbol{w}}_{t+1} - \bar{\boldsymbol{u}}_{t+1}||^2\right] \leq \frac{4d\eta_t^2 IG^2}{K2^{2m}}. \tag{67}$$

Then, we can know that D_3 becomes zero after taking the expectation from (66) and D_1 can be bounded by (67). We further obtain the upper bound D_2 as below

$$\begin{aligned} D_2 &= ||\bar{\boldsymbol{u}}_{t+1} - \bar{\boldsymbol{v}}_{t+1} + \bar{\boldsymbol{v}}_{t+1} - \boldsymbol{w}^*||^2 \\ &= \underbrace{||\bar{\boldsymbol{u}}_{t+1} - \bar{\boldsymbol{v}}_{t+1}||^2}_{E_1} + \underbrace{||\bar{\boldsymbol{v}}_{t+1} - \boldsymbol{w}^*||^2}_{E_2} + \underbrace{2\langle \bar{\boldsymbol{u}}_{t+1} - \bar{\boldsymbol{v}}_{t+1}, \bar{\boldsymbol{v}}_{t+1} - \boldsymbol{w}^* \rangle}_{E_3}. \end{aligned} \tag{68}$$

We leverage the result of the random scheduling from [12] to simplify (68) as follows

$$\mathbb{E}[\bar{\boldsymbol{u}}_{t+1}] = \bar{\boldsymbol{v}}_{t+1} \tag{69}$$

$$\mathbb{E}[\bar{\boldsymbol{v}}_{t+1} - \bar{\boldsymbol{u}}_{t+1}||^2] \leq \frac{4(N-K)}{K(N-1)}\eta_t^2 I^2 G^2. \tag{70}$$

We can see that E_3 will vanish due to (69). E_1 and E_2 can be upper bounded by (70) and Lemma 5, respectively. Therefore, we have

$$\begin{aligned} \mathbb{E}\left[||\bar{\boldsymbol{w}}_{t+1} - \boldsymbol{w}^*||\right]^2 &\leq \mathbb{E}\left[||\bar{\boldsymbol{v}}_{t+1} - \boldsymbol{w}^*||\right] + \frac{4d\eta_t^2 IG^2}{K2^{2m}} + \frac{4(N-K)}{K(N-1)}\eta_t^2 I^2 G^2. \\ &= (1-\mu\eta_t)\mathbb{E}\left[||\bar{\boldsymbol{w}}_t - \boldsymbol{w}^*||^2\right] + \eta_t^2\psi - \frac{\mu\eta_t d}{2^{2n}}, \end{aligned} \tag{71}$$

where

$$\psi = \sum_{k=1}^{N} \frac{\sigma_k^2}{N^2} + \frac{d}{2^{2n}} + 4(I-1)^2 G^2 + \frac{4dIG^2}{K2^{2m}} + \frac{4(N-K)}{K(N-1)} I^2 G^2. \tag{72}$$

In (71), we have $\frac{\mu\eta_t d}{2^{2n}}$, which is the quantization error from the local training. To upper bound (71) with this term, we use the fact that $\eta_t > \eta_t^2$ and obtain the following inequality:

$$\mathbb{E}\left[||\bar{\boldsymbol{w}}_{t+1} - \boldsymbol{w}^*||\right]^2 \leq (1-\mu\eta_t)\mathbb{E}\left[||\bar{\boldsymbol{w}}_t - \boldsymbol{w}^*||^2\right] + \eta_t^2 D, \tag{73}$$

where $D = \psi - \frac{\mu d}{2^{2n}}$. Since $\mathbb{E}\left[||\bar{\boldsymbol{w}}_t - \boldsymbol{w}^*||\right] \leq \frac{\beta^2 D}{(\beta\mu - 1)(t+\gamma)}$ satisfies (72) for $\eta_t = \frac{\beta}{t+\gamma}$ as shown in [22]. Then, we can obtain Theorem 1 from L - smoothness of the loss function using $\mathbb{E}[F(\bar{\boldsymbol{w}}_{t+1}) - F(\boldsymbol{w}^*)] \leq \frac{L}{2}\mathbb{E}\left[||\bar{\boldsymbol{w}}_{t+1} - \boldsymbol{w}^*||\right]^2$. Finally, we change the time scale to local iteration.

REFERENCES

[1] M. Kim, W. Saad, M. Mozaffari, and M. Debbah, "On the tradeoff between energy, precision, and accuracy in federated quantized neural networks," in *Proc. IEEE Int. Conf. Commun.*, Seoul, South Korea, May 2022.

[2] M. Chen, Z. Yang, W. Saad, C. Yin, H. V. Poor, and S. Cui, "A joint learning and communications framework for federated learning over wireless networks," *IEEE Trans. Wireless Commun.*, vol. 20, no. 1, pp. 269–283, Jan. 2021.

[3] R. Schwartz, J. Dodge, N. A. Smith, and O. Etzioni, "Green AI," *arXiv preprint arXiv:1907.10597*, 2019.

[4] H. B. McMahan, E. Moore, D. Ramage, S. Hampson, and B. A. Arcas, "Communication-efficient learning of deep networks from decentralized data," *arXiv preprint arXiv:1602.05629*, 2017.

[5] B. Moons, K. Goetschalckx, N. Van Berckelaer, and M. Verhelst, "Minimum energy quantized neural networks," in *Proc. of Asilomar Conf. on Signals, Systems, and Computers*, Pacific Grove, CA, USA, Apr. 2017.

[6] S. Savazzi, V. Rampa, S. Kianoush, and M. Bennis, "An energy and carbon footprint analysis of distributed and federated learning," *arXiv preprint arXiv:2206.10380*, 2022.

[7] N. H. Tran, W. Bao, A. Zomaya, M. N. H. Nguyen, and C. S. Hong, "Federated learning over wireless networks: Optimization model design and analysis," in *Proc. of IEEE Conf. on Computer Commun.*, Paris, France, May 2019.

[8] Z. Yang, M. Chen, W. Saad, C. S. Hong, and M. Shikh-Bahaei, "Energy efficient federated learning over wireless communication networks," *IEEE Trans. Wireless Commun.*, vol. 20, no. 3, pp. 1935–1949, Mar. 2021.

[9] Q. Zeng, Y. Du, K. Huang, and K. K. Leung, "Energy-efficient resource management for federated edge learning with cpu-gpu heterogeneous computing," *IEEE Trans. Wireless Commun.*, 2021, to appear.

[10] B. Luo, X. Li, S. Wang, J. Huangy, and L. Tassiulas, "Cost-effective federated learning design," in *Proc. of IEEE Conf. on Computer Commun.*, Vancouver, BC, Canada, May 2021.

[11] R. Balakrishnan, M. Akdeniz, S. Dhakal, and N. Himayat, "Resource management and fairness for federated learning over wireless edge networks," in *Proc. IEEE Workshop on Signal Process. Advances in Wireless Commun.*, Atlanta, GA, USA, May 2020, pp. 1–5.

[12] S. Zheng, C. Shen, and X. Chen, "Design and analysis of uplink and downlink communications for federated learning," *IEEE J. Sel. Areas Commun.*, vol. 39, no. 7, Jul. 2021.

[13] A. Reisizadeh, A. Mokhtari, H. Hassani, A. Jadbabaie, and R. Pedarsani, "Fedpaq: A communication-efficient federated learning method with periodic averaging and quantization," in *International Conference on Artificial Intelligence and Statistics*, Virtual Conference, Jun. 2020, pp. 2021–2031.

[14] J. Xu, W. Du, Y. Jin, W. He, and R. Cheng, "Ternary compression for communication-efficient federated learning," *IEEE Trans. Neural Netw.*, vol. 33, no. 3, pp. 1162–1176, Mar. 2022.

[15] Y. Yang, Z. Zhang, and Q. Yang, "Communication-efficient federated learning with binary neural networks," *IEEE J. Sel. Areas Commun.*, vol. 39, no. 12, pp. 3836–3850, Jan. 2021.

[16] N. Zhang and M. Tao, "Gradient statistics aware power control for over-the-air federated learning," *IEEE Trans. Wireless Commun.*, vol. 20, no. 8, pp. 5115–5128, Aug. 2021.

[17] I. Hubara, M. Courbariaux, D. Soudry, R. El-Yaniv, and Y. Bengio, "Quantized neural networks: Training neural networks with low precision weights and activations." *arXiv preprint arXiv:1609.07061*, 2016.

[18] S. Gupta, A. Agrawal, K. Gopalakrishnan, and P. Narayanan, "Deep learning with limited numerical precision," in *Proc. of International Conference on Machine Learning (ICML)*, Lille, France, Jul. 2015.

[19] S. Zhou, Y. Wu, Z. Ni, X. Zhou, H. Wen, and Y. Zou, "Dorefa-net: Training low bitwidth convolutional neural networks with low bitwidth gradients," *arXiv preprint arXiv:1606.06160*, 2018.

[20] B. Moons, D. Bankman, and M. Verhelst, *Embedded Deep Learning, Algorithms, Architectures and Circuits for Always-on Neural Network Processing*. Springer, 2018.

[21] E. Bjornson, E. A. Jorswieck, M. Debbah, and B. Ottersten, "Multiobjective signal processing optimization: The way to balance conflicting metrics in 5g systems," *IEEE Signal Processing Magazine*, vol. 31, no. 6, pp. 14–23, Nov. 2014.

[22] X. Li, K. Huang, W. Yang, S. Wang, and Z. Zhang, "On the convergence of fedavg on non-iid data," in *Proc. of International Conference on Learning Representations (ICLR)*, May 2020.

[23] Z. Yuchen, D. J. C., and W. M. J., "Communication-efficient algorithms for statistical optimization," *J. Mach. Learn. Res.*, vol. 14, no. 1, p. 3321–3363, Jan. 2013.

[24] I. Das and J. E. Dennis, "Normal-boundary intersection: A new method for generating the pareto surface in nonlinear multicriteria optimization problems," *SIAM journal on optimization*, vol. 8, no. 3, pp. 631–657, Aug. 1998.

[25] R. Wituła and D. Słota, "Cardano's formula, square roots, chebyshev polynomials and radicals," *Journal of Mathematical Analysis and Applications*, vol. 363, no. 2, pp. 639–647, Feb. 2010.

[26] D. P. Bertsekas, "Nonlinear programming," *Journal of the Operational Research Society*, vol. 48, no. 3, pp. 334–334, Jan. 1997.

[27] Z. Han, D. Niyato, W. Saad, T. Başar, and A. Hjørungnes, *Game Theory in Wireless and Communication Networks: Theory, Models, and Applications*. Cambridge University Press, 2011.

[28] L. M. Nguyen, P. H. Nguyen, M. van Dijk, P. Richtarik, K. Scheinberg, and M. Takac, "Sgd and hogwild! convergence without the bounded gradients assumption," in *Proc. of International Conference on Machine Learning (ICML)*, Stockholm, Sweden, Jul. 2018.

[29] X. Qian and D. Klabjan, "The impact of the mini-batch size on the variance of gradients in stochastic gradient descent," *arXiv preprint arXiv:2004.13146*, 2020.

[30] R. Yedida, S. Saha, and T. Prashanth, "Lipschitzlr: Using theoretically computed adaptive learning rates for fast convergence," *Applied Intelligence*, vol. 51, Mar. 2021.

[31] A. Øland and B. Raj, "Reducing communication overhead in distributed learning by an order of magnitude (almost)," in *Proc. of IEEE Int. Conf. Acoustics, Speech, and Signal Processing*, South Brisbane, QLD, Australia, 2015, pp. 2219–2223.

[32] R. Shwartz-Ziv and N. Tishby, "Opening the black box of deep neural networks via information," *arXiv preprint arXiv:1703.00810*, 2017.

[33] Y. Sarikaya and O. Ercetin, "Motivating workers in federated learning: A stackelberg game perspective," *IEEE Net. Lett.*, vol. 2, no. 1, pp. 23–27, Oct. 2020.